

THESIS FOR THE DEGREE OF LICENTIATE OF ENGINEERING

Aspects of Power Consumption in Coherent Fiber-Optical Communication Systems

Lars Lundberg



CHALMERS

Photonics Laboratory
Department of Microtechnology and Nanoscience (MC2)
CHALMERS UNIVERSITY OF TECHNOLOGY
Gothenburg, Sweden, 2017

Aspects of Power Consumption in Coherent Fiber-Optical Communication Systems

Lars Lundberg

© Lars Lundberg, 2017

Chalmers University of Technology
Department of Microtechnology and Nanoscience
Photonics Laboratory
SE-412 96 Göteborg
Sweden
Telephone: +46 (0)31-772 10 00

ISSN 1652-0769
Technical Report MC2-368

Printed in Sweden by Reproservice, Chalmers tekniska högskola, 2017

Aspects of Power Consumption in Coherent Fiber-Optical Communication Systems

Lars Lundberg

Photonics Laboratory
Department of Microtechnology and Nanoscience
Chalmers University of Technology
SE-412 96 Göteborg, Sweden

Abstract

The power consumption of coherent fiber-optical communication systems is becoming increasingly important, for both environmental and economical reasons. The data traffic on the Internet is increasing at a faster pace than that at which optical network equipment is becoming more energy efficient, which means that the overall power consumption of the Internet is increasing. In addition, wasted energy leads to higher costs for network operators, through increased electricity expenses but also because the heat generated in the equipment limits how closely it can be packed.

This thesis includes power consumption modelling, trade-off studies and investigations of novel schemes that may lead to an improved energy efficiency in future systems. In particular, the power consumption of optical amplifiers is modelled and connected to a performance model based on the Gaussian-noise model. Using these models, the trade-offs between amplifier power consumption and the choice of modulation format and forward-error-correction (FEC) scheme is studied. We find that 16-ary quadrature-amplitude modulation (16QAM) has a lower energy consumption per bit than quadrature phase-shift keying (QPSK) due to its higher spectral efficiency, and that using a shorter amplifier spacing to improve signal quality may be more energy efficient than using a powerful FEC.

Furthermore, the power consumption for a coherent link with minimal digital signal processing (DSP) is studied. We find that when the DSP is minimized, it accounts for below 10% of the power consumption, which is dominated by the optical components.

Finally, we demonstrate that the phase-coherence of optical frequency comb lines can be utilized to simplify the carrier-recovery by joint processing of multiple wavelength channels. We use the phase-drift from one wavelength channel to compensate the phase-drift of another one spaced up to ± 275 GHz away with negligible penalty.

Keywords: Fiber-optical communication, coherent detection, energy-efficiency, power consumption, optical amplifier, erbium-doped fiber amplifier, Raman amplification, digital signal processing, carrier-recovery, phase-tracking, optical frequency comb

List of papers

This thesis is based on the following appended papers:

- [A] **Lars Lundberg**, Peter A. Andrekson, and Magnus Karlsson, "Power Consumption Analysis of Hybrid EDFA/Raman Amplifiers in Long-Haul Transmission Systems," *Journal of Lightwave Technology*, vol. 35, no. 11, pp. 2132–2142, 2017.
- [B] **Lars Lundberg**, Christoffer Fougstedt, Per Larsson-Edefors, Peter A. Andrekson, and Magnus Karlsson, "Power Consumption of a Minimal-DSP Coherent Link with a Polarization Multiplexed Pilot-Tone," in European Conference on Optical Communication (ECOC), 2016.
- [C] **Lars Lundberg**, Mikael Mazur, Abel Lorences-Riesgo, Magnus Karlsson and Peter A. Andrekson, "Joint Carrier Recovery for DSP Complexity Reduction in Frequency Comb-Based Superchannel Transceivers," in European Conference on Optical Communication (ECOC), 2017.

Papers by the author not included in the thesis:

- [D] **Lars Lundberg**, Henrik Sunnerud, and Pontus Johannisson, "In-Band OSNR Monitoring of PM-QPSK Using the Stokes Parameters," in Optical Fiber Communication Conference (OFC), 2015, paper W4D.5.
- [E] **Lars Lundberg**, Pontus Johannisson, Erik Agrell, Magnus Karlsson, and Peter A. Andrekson, "Power consumption of hybrid EDFA/Raman amplified systems," in European Conference on Optical Communication (ECOC), 2015.

Acknowledgment

First of all, I would like to thank my supervisors Prof. Peter Andrekson and Prof. Magnus Karlsson for accepting me as a PhD-student and guiding me through the process. I also gratefully acknowledge guidance from Prof. Erik Agrell, Dr. Pontus Johannisson, Prof. Per Larsson-Edefors and Dr. Jochen Schröder.

My fellow project-member Christoffer Fougstedt deserves thanks for making me feel less lonely in this project, for teaching me about ASIC design and for generally being a friendly person.

The experimental work in this thesis would not have been possible without Dr. Abel Lorences-Riesgo, who has also been a nice office-mate, and Mikael Mazur, who also deserves thanks for sharing his enthusiasm for fiber-optical communication. In addition, my discussions with Attila Fülöp has been helpful for my understanding of DSP and in general very enjoyable.

I would also like to thank Sheila Galt for support on everything teaching-related and Jeanette Träff for handling everything administrative in such a good way.

In addition, all the people at the Photonics lab deserve thanks for making it such a friendly workplace. In particular, I am lucky enough to work at same place as Emanuel Haglund and Ewa Simpanen, whose friendship I have enjoyed throughout both my undergraduate and graduate education at Chalmers. Finally, I am grateful to all of my friends and family for their company and support.

Lars Lundberg

*Gothenburg
August 2017*

This work was financially supported by the Knut and Alice Wallenberg foundation

Abbreviations

ADC	Analog-to-digital converter	MCF	Multi-core fiber
ASE	Amplified spontaneous emission	MIMO	Multiple-input multiple-output
ASIC	Application-specific integrated circuit	MMA	Multi-modulus algorithm
BER	Bit-error rate	MUX	Multiplexer
BPS	Blind phase-search	MZM	Mach-Zehnder modulator
CD	Chromatic dispersion	NLI	Non-linear interference
CMA	Constant-modulus algorithm	OSNR	Optical signal-to-noise ratio
COP	Coefficient of performance	PBC	Polarization beam combiner
DAC	Digital-to-analog converter	PBS	Polarization beam splitter
DBP	Digital back-propagation	PMD	Polarization-mode dispersion
DCF	Dispersion-compensating fiber	PSK	Phase-shift keying
DD	Decision-directed	QPSK	Quadrature phase-shift keying
DEMUX	Demultiplexer	RDE	Radius-directed equalization
DSP	Digital signal processing	RF	Radio-frequency
EDF	Erbium-doped fiber	RX	Receiver
EDFA	Erbium-doped fiber amplifier	SDH	Synchronous digital hierarchy
FBG	Fiber-bragg grating	SDM	Spatial-division multiplexing
FEC	Forward error correction	SMF	Standard single-mode fiber
FIR	Finite impulse-response	SNR	Signal-to-noise ratio
FWHM	Full-width half-maximum	SONET	Synchronous optical networking
FWM	Four-wave mixing	SPM	Self-phase modulation
GMI	Generalized mutual information	TEC	Thermoelectric cooler
IQ	In-phase-quadrature	TIA	Transimpedance amplifier
ISI	Inter-symbol interference	TX	Transmitter
LD	Laser diode	WDM	Wavelength-division multiplexing
LO	Local oscillator	XPM	Cross-phase modulation

Contents

Abstract	i
List of papers	iii
Acknowledgment	v
Abbreviations	vii
1 Introduction	1
1.1 The role of coherent technologies	2
1.2 This thesis	2
1.2.1 Thesis outline	3
2 Coherent fiber-optical communication and power consumption	5
2.1 Building blocks	5
2.1.1 The laser	6
2.1.2 The modulator	6
2.1.3 The optical amplifier	7
2.1.4 The coherent receiver	8
2.1.5 Analog-to-digital conversion	8
2.1.6 Digital signal processing	9
2.1.7 Forward error correction	9
2.2 Transmission impairments	9
2.2.1 Chromatic and polarization-mode dispersion	10
2.2.2 Non-linear impairments	10
2.3 Modulation formats	11
	ix

3	Power consumption of optical amplifiers	13
3.1	Erbium-doped fiber amplifiers	13
3.1.1	Fundamental limits	14
3.1.2	The two-level model	15
3.1.3	Amplified spontaneous emission noise	16
3.2	Distributed Raman amplification	17
3.2.1	ASE noise and nonlinear effects in Raman systems	19
3.3	Power consumption model	20
3.4	System optimization	22
3.4.1	EDFA	22
3.4.2	Hybrid Raman amplification	23
4	Digital signal processing	25
4.1	Overview of DSP for coherent systems	25
4.1.1	Optical front-end correction	25
4.1.2	Chromatic dispersion	26
4.1.3	Clock recovery	26
4.1.4	Adaptive equalization	27
4.1.5	Carrier recovery	28
4.2	Implementation and power-consumption aspects	28
4.2.1	Power consumption	28
4.2.2	Relative power consumption of the steps in DSP for optical communications	29
5	Advanced methods for carrier recovery	31
5.1	Carrier frequency offset and phase-drift	31
5.2	Pilot-tone based carrier-recovery	32
5.3	Digital carrier-recovery methods	32
5.3.1	Frequency offset estimation	33
5.3.2	Feedback-based phase-tracking	33
5.3.3	The Viterbi-Viterbi algorithm	33
5.3.4	Blind phase search	34
5.3.5	Phase unwrapping and cycle slips	35
5.4	Joint carrier-recovery	36
5.4.1	Phase-locked multichannel systems	36
5.4.2	Algorithms for joint phase-tracking	37
5.4.3	Effects of optical delay	39
6	Future outlook	41

7 Summary of papers	43
Bibliography	45
Papers A–C	55

Chapter 1

Introduction

As of the time of this writing, August 2017, it is estimated that almost half of the world's population are Internet users [1]. As such they are also users of fiber-optical communication, which is a technology crucial for the network infrastructure supporting the Internet. The usage of fiber-optical links ranges from underwater cables spanning thousands of kilometers, transporting data between continents, to high-capacity networks in the datacenters of service providers.

There are several inventions that have enabled fiber optical communication and the growth of throughput in deployed systems. The low-loss optical fiber [2] and the laser [3] are fundamental for fiber-optical communication, and the invention of the erbium-doped fiber amplifier (EDFA) [4] extended the repeater-free reach and enabled the throughput to increase with wavelength-division multiplexing (WDM). More recently, coherent detection in combination with digital signal processing (DSP) [5] has enabled modulation formats with higher spectral efficiency. In addition, information theory, founded with Claude Shannons landmark paper [6], as well as error control coding [7, 8] are fundamental for the capacity of modern systems.

Altogether, the fiber capacity has increased several orders in the last decades. Lucky enough, the power consumption of the equipment has not seen the same increase, which has enabled the energy consumption per bit to decrease. For transatlantic cables, this decrease was estimated to be 20% annually [9]. However, the annual data traffic growth is estimated to be 40-50% [10], so the overall power consumption and energy use of the network infrastructure is increasing. There are several reasons to work to mitigate this trend. Maybe the most obvious one is the effects the use of fossil energy has on our planet [11], but there are also more pragmatical reasons to improve energy efficiency. Apart from the obvious cost of energy that can be seen on any network operator's electricity bill, wasted energy takes the form of heat which

requires cooling and set limits to how dense equipment can be packed [12]. Since space is a costly resource, this provides an additional incentive to improve energy efficiency.

This has created a need for a changed approach to development in the area of fiber optics. While the traditional approach has been to focus on performance and cost when designing systems, the systems of tomorrow need to be designed with an equal focus on power consumption. The work in this thesis contributes to this design paradigm.

1.1 The role of coherent technologies

This focus of this work is on fiber-optical links using coherent detection. The strength of coherent detection is that it enables detection of the full optical field, which has the advantages that it enables the use of higher order modulation formats and that signal impairments can be compensated for with DSP. However, coherent transceivers have a significantly higher complexity and power consumption than transceivers for intensity-modulated signals. Therefore, coherent technologies have traditionally mainly been used in long-haul, high capacity links. Due to the large investments involved in e.g. submarine cables, and the relatively low number of installed links, the sensitivity to transceiver cost and power consumption is relatively low in this area. However, the use of coherent detection also in shorter links is on the rise—mainly in metro networks [13], but also in inter-datacenter interconnects [14]. These applications are more sensitive to cost and power consumption.

1.2 This thesis

The main topic of this thesis is power consumption in coherent fiber-optical communication systems. The overarching goal is to contribute to an increased energy efficiency of such systems. This problem is approached on the link level, as opposed to optimizing energy efficiency on the lower component level, or on the higher network level. The papers included in this thesis falls into two categories: Modeling and understanding power consumption tradeoffs [Paper A–B], and investigating possibly power saving transmission schemes [Paper C].

In [Paper A], the power consumption of optical amplifiers is modelled, and the tradeoff between power consumption and signal quality in terms of optical signal-to-noise ratio (OSNR) is investigated. The amplifier power consumption model includes both EDFAs and distributed Raman amplification. The connection between the OSNR and the power consumption enables analysis of the implications different

modulation formats and forward error correction (FEC) schemes has on the amplifier power consumption.

In [Paper B] we investigate a minimal-DSP link, where length-dependent transmission impairments are absent, and polarization demultiplexing and carrier-recovery are aided by an optical pilot-tone.

In [Paper C] we investigate the possibilities of utilizing the phase coherence of optical frequency combs to improve the efficiency of carrier-recovery algorithms in multi-wavelength receivers.

1.2.1 Thesis outline

This thesis is organized as follows: Chapter 2 provides an overview over coherent fiber-optical communication systems and their power consumption, discussing how the basic building blocks and phenomena contribute to the power consumption. Chapter 3 is devoted to the power consumption of the two most common optical amplification technologies, EDFAs and Raman amplification. We develop power consumption models from basic amplifier models and discuss system-wide trade-offs between amplifier power consumption and signal quality. In Chapter 4 the basic DSP functions needed in coherent systems are described and the challenges of modelling DSP power consumption are discussed. The topic of Chapter 5 is carrier-recovery and how optical methods can be combined with DSP to achieve a more efficient carrier recover. Finally, Chapter 6 provides a future outlook.

Chapter 2

Coherent fiber-optical communication and power consumption

This chapter covers several aspects of coherent fiber-optical communication systems. The purpose is to provide an overview over the basic building blocks, their working principle and impact on power consumption. In addition, we briefly discuss important transmission impairments, how they can be compensated for and the associated power consumption.

2.1 Building blocks

A telecommunication system, such as a fiber-optical link contains three essential parts: A *transmitter* that takes information and converts into a physical signal, a *transmission medium* that carries the signal, and a *receiver* that converts the signal back to usable data. In a fiber-optical link, the signal is carried on a lightwave, through an optical fiber, which is the transmission medium. However, the transmitter and receiver technology may differ between different kinds of fiber-optical systems.

In this thesis we consider coherent systems where the full optical field, i.e. both amplitude and phase on both polarizations is utilized to transmit information. The important building blocks of a coherent transmitter is the laser, which provides the carrier lightwave, and the modulator, which encodes the data onto the signal. Optical amplifiers can be considered to be part of the transmission medium. In the coherent

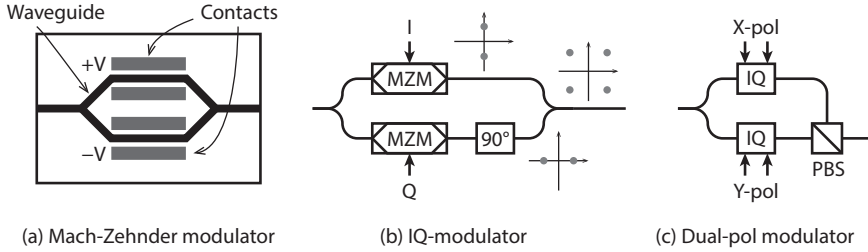


Figure 2.1: Principle of (a) an MZM (b) an IQ-modulator and (c) a dual-polarization IQ-modulator.

receiver, the signal is detected with the help of a local oscillator (LO) laser, and processed digitally to compensate impairments.

2.1.1 The laser

In coherent systems, a laser is needed both in the transmitter as a carrier and as an LO in the receiver. Typically, diode lasers are used. Important properties of lasers in coherent communication systems are output power, wavelength stability and linewidth. To assure wavelength stability, active cooling with thermoelectric coolers is used, which should be included when considering the power consumption. This is described in detail in Section 3.3. A tunable laser suitable for use in coherent systems can consume several watts [15], which is a considerable part of the transmitter power consumption [16]. However, in a transceiver, the same laser can often be used both as a carrier for the transmitter part and LO for the receiver part, thus sharing the power consumption.

2.1.2 The modulator

Coherent systems use optical in-phase-quadrature (IQ) modulators to modulate the full optical field. Although a single dual-drive Mach-Zehnder modulator can be used for quadrature modulation [17], to achieve independent modulation of the in-phase and quadrature dimensions, optical IQ-modulators are constructed with parallel Mach-Zehnder modulators (MZM). Mach-Zehnder modulators are based on placing two phase modulators in an interferometric structure, like in Fig. 2.1(a). If opposite voltages are applied to the phase modulators, the amplitude of the output of the MZM can be modulated between -1 and 1 following the real axis in the transitions. To achieve modulation over the whole complex plane, two MZMs are combined with a 90° phase shift (Fig. 2.1(b)). Finally, to modulate the full optical field, i.e.

both polarizations, the output from two MZM-based IQ-modulators are combined with a polarization beam-combiner (PBC) (Fig. 2.1(c)).

Important parameters for modulators are bandwidth, drive voltage and insertion losses, which are all related. The drive voltage is characterized by the voltage to achieve a phase shift of 180° (or π) in the phase modulators, written V_π . For the MZM described above, this corresponds to the voltage needed to go between -1 and 1 . High-speed phase modulators are often based on the travelling-wave design [17, Ch. 2], where the electrodes are designed as a transmission line alongside the optical waveguide. In a travelling-wave modulator, the light is modulated as it travels through the waveguide. To lower the V_π it is desirable to have a long interaction length between the electrical signal and the light, but due to difference in propagation speed between the electrical signal and the light, a long interaction length will reduce the modulation bandwidth of the modulator [17, Ch. 2]. In addition, long interaction lengths will increase losses both in the electrical transmission line and the optical waveguide [18].

The power consumption of the modulator has two main components. First, high insertion losses require high optical power from the transmitter laser, or even booster amplifiers. Second, a high drive voltage leads to a high electrical power consumption. The electrical power is not consumed in the modulation process itself, but is rather dissipated in the 50Ω terminations or in transmission line losses, and is proportional to V_π^2 . In [16], it is estimated that the modulator constitutes around 35% of the transmitter power consumption.

Phase modulators can be constructed from several different materials, but the most established today is lithium-niobate (LiNbO_3), where phase-modulation is achieved through the electro-optic effect. Other possible materials are indium phosphide (InP) and silicon. Modulators based on InP can be integrated with other InP optical components, such as tunable lasers, receivers and arrayed waveguide gratings [19]. Silicon-based modulators has the advantage of being possible to integrate with silicon electronics [18].

2.1.3 The optical amplifier

To manage fiber losses optical amplification is used, most commonly in the form of lumped erbium-doped fiber amplifiers (EDFAs). The optical amplifiers are also the most important noise source, as they inherently add amplified spontaneous emission (ASE) noise to the signal. The EDFAs are inserted with a spacing of between 50 km and 100 km. Alternatively, the transmission fiber can be used as amplification medium through stimulated Raman scattering. Since the amplification takes place along the transmission fiber, this is referred to as distributed amplification. The main reason

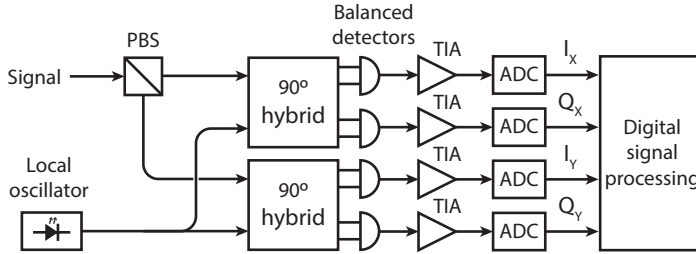


Figure 2.2: A phase- and polarization-diversity coherent receiver.

for using Raman amplification is its beneficial noise properties. Optical amplifiers are covered in detail in Chapter 3.

2.1.4 The coherent receiver

Today, the term coherent receiver usually refers to a phase- and polarization-diversity coherent receiver, that is capable of detecting both phase and amplitude of the optical field. Figure 2.2 shows a schematic of such receiver. The optical signal is split into orthogonal polarization states with a polarization beam splitter (PBS) and each of the polarizations is mixed with an LO laser in a 90° hybrid. The signal and LO is detected with balanced photodetectors. Optical 90° hybrids can be realized in several ways [20]. Typically, the receiver is operated in intradyne mode, which means that the LO laser is kept at approximately, but not exactly, the same frequency as the signal. Then there will be a remaining frequency difference between the signal and the LO that needs to be tracked using digital signal processing.

The signal from the photodetectors can be amplified with transimpedance amplifiers (TIAs) before analog-to-digital conversion. Power consumption of photodiode bias and TIAs is a comparably small part of the receiver power consumption [16].

2.1.5 Analog-to-digital conversion

The analog-to-digital converters (ADCs) are responsible for converting the analog signal from the balanced detectors to fixed-point digital signals suitable for digital signal processing (DSP). For fiber-optical systems, the most suitable technology is based on time-interleaved successive approximation [21]. The power consumption of this ADC technology is approximately linearly dependent on the ADC bit resolution, which determines the number of quantization levels, and the sampling rate [22].

2.1.6 Digital signal processing

DSP is an essential part of coherent optical communication systems, and also a major power consumer. Chapter 4 covers DSP in detail.

2.1.7 Forward error correction

Often, a signal is considered error free if the bit-error rate (BER) is below 10^{-15} . To achieve such low BERs, modern fiber optical communication systems rely on forward error correction (FEC), where a small redundancy added to the signal is traded against a significantly higher tolerance to noise and other impairments. FEC codes require encoding and decoding that may consume considerable amounts of power [16, 23].

There are two main categories of error-correcting codes, hard-decision codes and soft-decision codes. Hard-decision codes are decoded after a symbol decision has been made, while soft-decision codes perform decoding based on soft information about the received samples. Typically, soft-decision codes have a higher error-correcting capability at the cost of a higher decoding complexity and power consumption. Hard-decision codes can be described with the maximum pre-FEC BER allowed to achieve a post-FEC BER of 10^{-15} , and this FEC performance measure is often used for soft decision codes as well. However, for soft-decision codes, pre-FEC BER has been shown to be a poor predictor for post-FEC BER [24]. Instead, the generalized mutual information (GMI) can be used.

The overall trend is that a higher error-correcting capability leads to a higher power consumption. Since the power consumption of the line amplifiers can be reduced if the OSNR is lower, there is possibly a trade-off between the FEC power consumption and the power consumption of the amplifiers. Indeed, in [Paper A] we find that there are cases where the combined FEC and amplifier power consumption can be lowered by using a more powerful FEC and operating the system at a lower OSNR. However, specific details of the code type, design and implementation has also a big impact on the power consumption, so one should be careful before drawing wide conclusions from this example.

2.2 Transmission impairments

Propagation in the fiber will distort the signal. These distortions can be divided into two main categories, linear impairments and non-linear impairments. This section will discuss these impairments and how they can be compensated for. In addition,

the power consumption related to the compensation of the impairments is briefly covered.

2.2.1 Chromatic and polarization-mode dispersion

Chromatic dispersion is caused by the frequency dependence of the propagation constant in the fiber. This is caused by a combination of material dispersion and waveguide dispersion. Chromatic dispersion causes inter-symbol interference (ISI) and if it is not compensated for, it severely limits the transmission reach. Compensation can be performed both in the optical domain or electronically using DSP. The most common optical method is dispersion-compensating fiber (DCF), which has been designed to have a dispersion parameter with an opposite sign to that of standard single mode fiber (SMF). Another method is fiber Bragg gratings (FBG). Optical dispersion compensation contributes to the power consumption by introducing losses that need to be compensated with optical amplification [25]. Since FBGs have lower losses than DCF [26], they are a more power efficient choice. DSP-based electronic dispersion is covered in more detail in Section 4.1.2. If used, it is one of the major power consumers in the receiver [16].

Polarization-mode dispersion (PMD) is caused by fiber birefringence, which leads to a polarization dependent propagation constant. The birefringence is caused by small deviations of the fiber core geometry along the fiber. Since the effect PMD has on the signal varies depending on the polarization, and the polarization drifts with time, PMD is a time dependent impairment. From a signal processing point of view, PMD causes a frequency dependent crosstalk between the polarizations, and can thus be compensated for with a 2×2 MIMO-equalizer. Since PMD varies with time, this equalizer needs to be adaptive.

2.2.2 Non-linear impairments

In addition to the previously discussed linear impairments, the non-linear power dependence of the refractive index of the optical fiber causes transmission impairments. The refractive index of optical fiber has a quadratic dependence on optical power, which is known as the Kerr effect. Since the light is highly confined in the core, which leads to high power densities, non-linear effects are important even though silica is not highly non-linear. Through the power dependence of the refractive index, the signal will distort itself through self-phase modulation (SPM) and also interact with other wavelength channels and noise through cross-phase modulation (XPM) and four-wave mixing (FWM).

Non-linear transmission impairments can be partly compensated using digital back-propagation (DBP) [27], but this involves solving the non-linear Schrödinger

equation which is computationally intensive. While DBP has been extensively analyzed from a performance point of view [28], only a few investigations of implementation aspects exist [29, 30].

In long-haul links without inline dispersion compensation, nonlinear effects can often be treated as Gaussian noise [31, 32]. The reason for this description to be valid is that the signal distortion caused by chromatic dispersion causes the nonlinear interference to resemble Gaussian noise. This model is widely known as the *Gaussian-noise model* or *GN model*. The underlying theory has been described in e.g. [31, 32]. The fundamental result is that an additional term S_{NLI} proportional to the cube of signal power is added to the noise power spectral density. The optical signal-to-noise ratio (OSNR) is then

$$\text{OSNR} = \frac{P_s}{(S_{\text{ASE}} + S_{\text{NLI}})\Delta\nu} = \frac{P_s}{(S_{\text{ASE}} + k_{\text{NLI}}P_s^3)\Delta\nu}, \quad (2.1)$$

where P_s is the signal launch power, S_{ASE} is the amplifier noise power spectral density, $\Delta\nu$ is the noise bandwidth (usually corresponding to 0.1 nm) and k_{NLI} is a proportionality constant that depend on fiber properties and signal spectra of the whole system.

Another important results from this model is that it gives a formal expression for the optimal signal power that gives the highest OSNR, which is when ASE and nonlinearities balance each other. This is given by

$$P_{\text{opt}}^s = \left(\frac{S_{\text{ASE}}}{2k_{\text{NLI}}} \right)^{1/3}. \quad (2.2)$$

This optimum point is in many cases used in combination with the Shannon capacity as a measure of the maximum possible capacity of a fiber system. However, this is not actually the capacity of the fiber channel. Instead it is a lower bound on it [33], whereas the actual capacity remains unknown.

2.3 Modulation formats

Coherent transmission enables the use of quadrature amplitude modulation (QAM) formats, illustrated in Fig. 2.3. Quadrature phase-shift keying (QPSK, or 4QAM) and 16QAM is today available in commercial coherent transceivers [12], and even higher order formats are expected to be available in the future.

The choice of modulation format affects the power consumption in several ways. Higher order modulation formats are more sensitive to noise, which may lead to higher power consumption in amplifiers [Paper A] and FEC. They also require higher

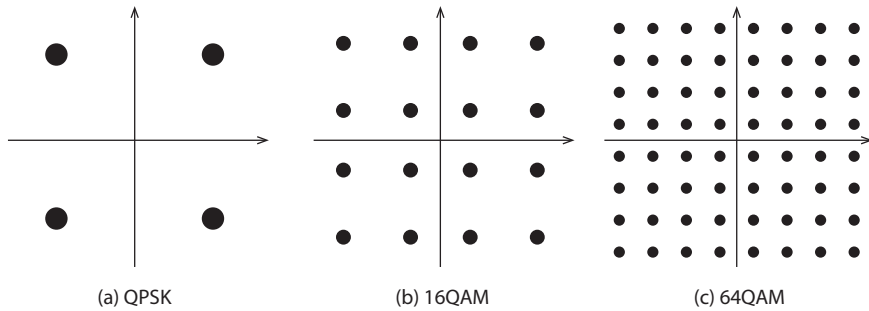


Figure 2.3: Constellations of three modulation formats.

bit-resolution which increase power consumption of ADCs and all DSP. In addition, higher order modulation formats are also more sensitive to impairments such as phase-noise and thus require more complex phase-tracking algorithms. However, due to the increased spectral efficiency, the power consumption per bit may be unaffected or even lowered [16, 23], [Paper A].

Chapter 3

Power consumption of optical amplifiers

Optical amplifiers are a fundamental part of long-haul optical communication systems and a major power consumer [16]. They are also the most important noise source, and the choice of amplification scheme has significant impact on the signal quality at the receiver. To be able to investigate the trade-offs between signal quality and power consumption, this needs to be considered when modelling amplifier power consumption. In this chapter the power consumption of the two most common optical amplification technologies, erbium-doped fiber amplifiers (EDFAs) and distributed Raman amplification, is described starting from fundamental amplifier models.

Both EDFAs and Raman amplifiers have in common that they provide optical gain by pumping an amplification medium with a high power optical beam. While EDFAs use erbium-doped fiber (EDF) as amplification medium, Raman amplification can be achieved in standard single mode fiber (SMF). Parts of the power consumption of optical amplifiers is directly proportional to the pump power, so the following sections will be spent connecting the required pump power to other important amplifier properties such as gain and output power.

3.1 Erbium-doped fiber amplifiers

The erbium-doped fiber amplifier is the dominant amplifier technology used in long-haul fiber-optical communication systems. The amplification is achieved through sti-

mulated emission, which is the process where a photon stimulates an atomic energy transition. The energy is released in the form of a photon with identical wavelength, phase, polarization and propagation direction as the incident photon. Er^{3+} ions are used since they have an atomic energy transition matching the telecommunication wavelength of 1550 nm. To provide gain, there must be population inversion, i.e. a majority of the ions need to be in the excited state.

In amorphous silica, the energy levels of the Er^{3+} ions are broadened to bands, providing gain over both the C- and L-band (1530–1565 nm and 1565–1625 nm respectively). Population inversion can be achieved by optical pumping, either at 980 nm or at 1480 nm. Pumping at 980 nm a third energy level, while 1480 nm corresponds to the upper parts of the same energy band that is providing amplification.

3.1.1 Fundamental limits

The efficiency with which the pump power is converted into signal power is fundamentally limited by photon number conservation, i.e. the most efficient case corresponds to when all pump photons are converted into signal photons. Then, the photon flux (the number of photons per second) at the output needs to equal the photon flux at the input, giving

$$\phi_{\text{out}}^s = \phi_{\text{in}}^s + \phi_{\text{in}}^p, \quad (3.1)$$

where ϕ_{out}^s and ϕ_{in}^s are the photon fluxes of the signal at the output and input of the amplifier and ϕ_{in}^p is the photon flux of the pump at the input. By observing that the photon flux can be written in terms of the optical power P like $\phi = P\lambda/(hc)$, where λ is the optical wavelength, h is the Planck constant and c is the speed of light, this equation can be rewritten

$$P_{\text{in}}^p = \frac{\lambda_s}{\lambda_p} (P_{\text{out}}^s - P_{\text{in}}^s), \quad (3.2)$$

where P_{out}^s and P_{in}^s are the signal powers at the output and input of the amplifier and P_{in}^p is pump power at the input. This shows that if all pump photons are converted to signal photons, the pump power needed will be proportional to the power added to signal. The maximum efficiency corresponds to the ratio between the pump and signal wavelengths. Assuming a signal wavelength of 1550 nm, this corresponds to a power conversion efficiency of 63% and 95% for pump wavelengths of 980 nm and 1480 nm respectively.

Despite its simplicity, as we will show in the next section, the general behavior of the pump and signal power dependence is well described by this model for typical uses of EDFAs in communication links, provided that the wavelength ratio is

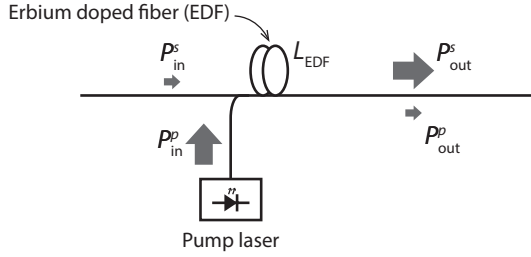


Figure 3.1: Schematic of a basic EDFA, with one co-propagating pump.

replaced with a non-ideal power conversion efficiency η_{PC} . The model then becomes

$$P_{in}^p = \frac{1}{\eta_{PC}} (P_{out}^s - P_{in}^s) \quad \text{where} \quad \eta_{PC} < \frac{\lambda_p}{\lambda_s}. \quad (3.3)$$

We will refer to this model as the *added-power model*. By observing that $P_{out}^s = G \cdot P_{in}^s$ it becomes

$$P_{in}^p = \frac{P_{in}^s}{\eta_{PC}} \left(1 - \frac{1}{G} \right). \quad (3.4)$$

For large amplification the pump power has only a weak dependence on the gain. Instead, it is directly proportional to the output power of the EDFA.

3.1.2 The two-level model

To further understand in which cases we can use the added-power model from the previous section, we will study the commonly used two-level model, which was introduced by Saleh et al. in 1990 [34]. The two-level model, as its name implies, models the EDFA system as having two energy levels. Out of the two pump wavelengths mentioned earlier, only the 1480 nm case is an actual two-level, but the model also describes the 980 nm pump system well, even though this pumping scheme involves three energy levels. The reason is that the upper energy level has a much shorter lifetime than the middle one, so at any time the population of the upper level is negligible.

The two-level model relates the input and output powers of any number of pump and signal beams, propagating in either direction in the erbium-doped fiber (EDF). The two-level model is only valid assuming that the gain is not saturated by amplified spontaneous emission (ASE) and ignores the impact of noise power, which can grow

to values comparable or even larger than the signal power. However, according to Saleh et al. [34] ASE can be safely neglected for gains less than 20 dB or input powers above -20 dBm. Nevertheless, the two-level model can also be extended to include ASE noise [35].

The process of solving the two-level model for one pump beam and one signal beam is described in [36, Ch. 5]. This situation is illustrated in Fig. 3.1. With this solution, the pump power can be written as a function of the input and output signal power,

$$P_{\text{in}}^p - P_{\text{out}}^p = \frac{\lambda_s}{\lambda_p} \left(P_{\text{out}}^s - P_{\text{in}}^s + P_{\text{IS}}^s \left(\ln \frac{P_{\text{out}}^s}{P_{\text{in}}^s} + \alpha_s L_{\text{EDF}} \right) \right) \quad (3.5)$$

$$= \frac{\lambda_s}{\lambda_p} \left(P_{\text{out}}^s \left(1 - \frac{1}{G} \right) + P_{\text{IS}}^s (\ln G + \alpha_s L_{\text{EDF}}) \right). \quad (3.6)$$

Here we have introduced the attenuation constant α_s and the intrinsic saturation power P_{IS}^s . They are defined as

$$\alpha_s = \rho \Gamma_s \sigma_s^a, \quad (3.7)$$

$$P_{\text{IS}}^s = \frac{Ah\nu_s}{(\sigma_s^e + \sigma_s^a)\tau\Gamma_s}, \quad (3.8)$$

where ρ is the erbium ion density, Γ_s is the signal mode overlap with the erbium ions, σ_s^a and σ_s^e are the absorption and emission cross-sections of erbium at the signal wavelength, A is the cross-sectional area of the beam and τ is the upper-state lifetime. For a typical EDF P_{IS}^s is less than 0.5 mW in the C-band, based on EDF parameters found in [36, Ch. 6].

The two-level model is approximately equivalent to the the added-power model provided that most of the pump power is absorbed in the EDF ($P_{\text{out}}^p \ll P_{\text{in}}^p$) and and that the signal output power is much larger than the intrinsic saturation power ($P_{\text{IS}}^s \ll P_{\text{out}}^s$). The first condition can be fulfilled by optimizing the EDF length, which is typically done in a well designed EDFA, and the second condition is typically fulfilled for a fully loaded wavelength-division multiplexed (WDM) system. In Fig. 3.2 the two-level model and the added-power model are compared for two different output powers. The power conversion efficiency in the added-power model is assumed to be ideal, i.e. $\eta_{\text{PC}} = \lambda_p/\lambda_s$, which leads the model to underestimate the required pump power.

3.1.3 Amplified spontaneous emission noise

In an EDFA, noise is added to the signal through spontaneous emission. This noise is then amplified by the stimulated emission process, which leads to amplified spon-

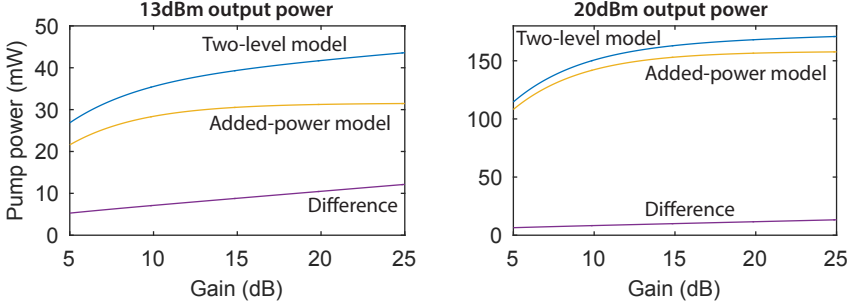


Figure 3.2: Required pump power as a function of gain for the two-level model and the added-power model for two different output powers. Ideal power conversion efficiency is assumed in the added-power model, i.e. $\eta_{PC} = \lambda_p/\lambda_s$. The pump and signal wavelengths are 980 nm and 1550 nm respectively and the EDF parameters are taken from [36, Ch. 6]. The EDF length is optimized for every gain value.

taneous emission (ASE). In a typical system, the ASE does not have any significant impact on the power consumption of the amplifiers, but it has a profound impact on the signal quality. Any noise added to the signal stays and is amplified together with the signal in any subsequent amplifiers, leading to ASE being one of the main transmission-reach-limiting factors. The power spectral density of the ASE can be written [37]

$$S_{ASE} = n_{sp} h \nu_0 (G - 1), \quad (3.9)$$

where h is the Planck constant, G is the amplifier gain, ν_0 is the frequency of the signal being amplified and n_{sp} is the spontaneous emission factor. The latter is also known as the population-inversion factor, and can be written

$$n_{sp} = \frac{N_2}{N_2 - N_1} > 1, \quad (3.10)$$

where N_1 and N_2 are the populations of the atomic ground and excited states respectively.

3.2 Distributed Raman amplification

Raman amplification utilizes stimulated Raman scattering to provide optical gain. Its use in modern optical communication systems is mainly due to two important properties that may be advantageous. The first one is that the transmission fiber can be

used as the amplification media, enabling distributed amplification which has beneficial noise properties. The other property is that the absolute spectral position of gain spectrum is defined by the wavelength of the pump. In silica fiber, the FWHM bandwidth is nearly 6 THz with a peak at 13.2 THz from the pump [38]. Since the pump wavelength determines the position of the gain spectrum, broadband amplification can be achieved by using several different-wavelength pumps.

While the basic concept of Raman amplification is similar to that of EDFAs, i.e. power is transferred from a higher energy pump wave to the signal, distributed Raman amplification is typically operated in a regime widely different from that of EDFAs. Compared to an EDFA, Raman amplification has a low power conversion efficiency, which results in most of the pump power being lost to losses in the fiber or still remaining at the output of the span.

Distributed Raman amplification can be either backward or forward pumped, or a combination of the two. The pumping schemes determine the evolution of the signal power as well as the noise properties. Since the signal power is maintained at a higher level, forward pumping has better noise properties than backward pumping. However, it suffers worse from other impairments such as pump noise transfer and nonlinear transmission impairments [39]. In addition, Raman amplification is also commonly combined with lumped EDFAs, so called hybrid amplification.

In general, Raman amplification can be described by a set of coupled differential equations that needs to be solved numerically [40]. However, if the signal power is much smaller than the pump power, the normalized signal power evolution is

$$\Gamma(z) = \frac{P_s(z)}{P_s(0)} = \exp\left(g_R \int_0^z P_p(\zeta) d\zeta - \alpha_s z\right), \quad (3.11)$$

where $P_s(z)$ and $P_p(z)$ are the signal and pump power evolutions along the fiber and g_R is the Raman gain coefficient, which is related to the cross section of spontaneous Raman scattering. For a span length of L the pump power evolution is $P_p^{\text{in}}(z) = \exp(-\alpha_p z)$ for forward pumping and $P_p^{\text{in}}(z) = \exp(-\alpha_p(L-z))$ for backward pumping. In the above equations, α_s and α_p are the signal and pump attenuation factors respectively.

The total Raman gain is conveniently expressed as the *on-off gain*, which is the ratio of the signal power at the output of the span with the Raman pump turned on and the signal power without Raman gain,

$$G_R = \Gamma(L)e^{\alpha_s L} = \exp(g_R P_p(0)L_{\text{eff}}), \quad (3.12)$$

where

$$L_{\text{eff}} = \frac{1 - e^{-\alpha_p L}}{\alpha_p} \quad (3.13)$$

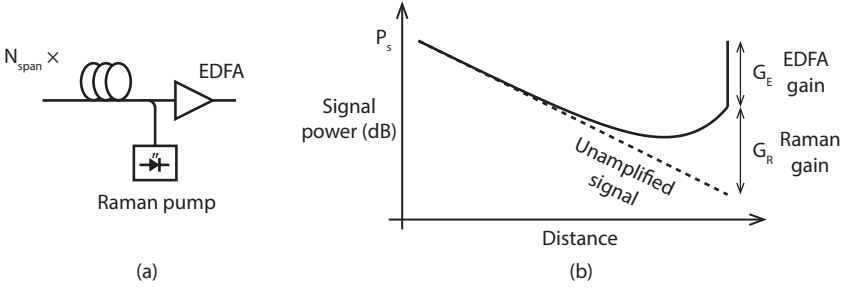


Figure 3.3: (a) Basic schematic of backwards-pumped hybrid EDFA/Raman amplification (b) The signal power evolution along the span for the system in (a).

is the Raman effective length. Thus, the pump power has a logarithmic dependence on the gain.

3.2.1 ASE noise and nonlinear effects in Raman systems

The ASE at the output of a Raman amplified span is described by

$$S_{\text{ASE,R}} = n_{\text{sp,R}} h \nu_0 g_R \Gamma(L) \int_0^L \frac{P_p(z)}{\Gamma(z)} dz, \quad (3.14)$$

where $n_{\text{sp,R}}$ is the Raman spontaneous emission factor which among other things depend on the temperature and the Raman shift. For a typical SMF at room temperature $n_{\text{sp,R}} = 1.13$ in the C-band [40, p. 50].

Distributed Raman amplification is often used together with EDFA-based lumped amplification to improve the optical signal-to-noise ratio (OSNR) and handle long spans. For backwards pumped Raman, since the amplification takes place mostly in the end of the fiber span, the reduction of noise power is almost independent of span length. This means that the OSNR improvement due to Raman amplification mostly depends on the Raman pump power. This is further discussed in [Paper A].

The Gaussian-noise (GN) model for non-linear interference described in Section 2.2 has been extended to cover also Raman amplified systems [41]. In the general case the signal power evolution needs to be integrated over the whole span, which is not always trivial. However, by approximating the signal power evolution with simple exponential functions it becomes easier [42]. In fact, for backwards pumped hybrid Raman, the effect of the changed power evolution can be neglected for lower Raman gains, and S_{NLI} can be calculated as for a system without distributed amplification. Pelouch [42] states that this is acceptable if the output power from the span

is more than 13 dB below the maximum power within the span, and Curri et al. [39] defines this region as when Raman amplification contributes with less than 60% of the total gain in dB.

3.3 Power consumption model

Generally, pump laser diodes are used for both EDFAs and Raman amplification. The power consumption can be modeled as being linearly dependent on the optical power input to the fiber

$$P_e = \frac{1}{\eta} P_p + P_{\text{mm}}, \quad (3.15)$$

where η is a power conversion efficiency that include all sources of inefficiencies that are proportional to the pump power, and P_{mm} is a constant power consumption term to account for monitoring and management circuitry for the amplifier.

The factor η includes several sources of inefficiencies. Firstly, the coupling of pump power into the amplification fiber has a limited efficiency. Secondly, the pump laser has some electrical-to-optical power conversion efficiency and thirdly, diode lasers in many cases require active cooling with thermoelectric coolers (TECs) to maintain wavelength stability, whose power consumption can be included in an efficiency factor.

To find the conversion efficiency η , we start by writing the power consumption as the sum of the power consumption of the laser diode and the TEC

$$P_{\text{pump}}^e = P_{\text{LD}}^e + P_{\text{TEC}}^e, \quad (3.16)$$

where the power consumption of the laser diode is proportional to the optical output power, $P_{\text{LD}}^e = P_{\text{LD}}^o / \eta_{\text{LD}}$, and the power consumption of the TEC is proportional to the heat removed, $P_{\text{TEC}}^e = Q_{\text{LD}} / k_{\text{TEC}}$. Here k_{TEC} is the TEC coefficient of performance (COP) [43]. The heat removed with the TEC can be assumed to be equal to the electrical power not converted to optical power in the laser diode and thus found by subtracting the optical output power from the laser diode power consumption, so

$$P_{\text{TEC}}^e = \frac{1}{k_{\text{TEC}}} (P_{\text{LD}}^e - P_{\text{LD}}^o) = \frac{1}{k_{\text{TEC}}} \left(\frac{1}{\eta_{\text{LD}}} - 1 \right) P_{\text{LD}}^o. \quad (3.17)$$

This leads to the the total power consumption

$$P_{\text{pump}}^e = \left(\frac{1}{\eta_{\text{LD}}} + \frac{1}{k_{\text{TEC}} \eta_{\text{LD}}} - \frac{1}{k_{\text{TEC}}} \right) P_{\text{LD}}^o \quad (3.18)$$

which is proportional to the optical output power. To include also the coupling into the amplification fiber we can replace the laser diode output power with the pump power needed in the amplification fiber

$$P_{\text{pump}}^e = \frac{1}{\eta_c} \left(\frac{1}{\eta_{\text{LD}}} + \frac{1}{k_{\text{TEC}} \eta_{\text{LD}}} - \frac{1}{k_{\text{TEC}}} \right) P_{\text{pump}}^o, \quad (3.19)$$

where η_c is the coupling efficiency.

The TEC COP depends on the temperature difference between the hot and the cold side of the TEC. For low temperature differences it can be above 100%. However, the temperature in equipment huts can be as high as 75°C while the laser diode should be kept at 25°C. In this worst case temperature difference of 50 K, the typical COP is only 17% [44]. Although Raman pump laser diodes can have a power conversion efficiency of 25% [45], when this combined with the other inefficiencies and input into Eq. (3.19) an overall electrical to coupled pump power efficiency of 3% is found. Here, a coupling efficiency of 1.5 dB was assumed. EDFA pump lasers can have a higher efficiency since they do not necessarily require active cooling (e.g. [46]). For example, in [47] an overall electrical to signal power conversion efficiency of 5% was used. This included also the power conversion between pump and signal.

In addition to the power consumption of the pump lasers, which is directly related to the operating conditions of the amplifier, such as output power and gain, optical amplifiers also include control and management circuitry that consumes power. This power consumption, which will be referred to as the *monitoring and management* can be modelled as being independent of the operating conditions of the amplifier, i.e. a constant term added for each amplifier unit. If just one amplifier is studied the value of the monitoring and management power consumption does not affect the optimum point, but in a system optimization scenario where the number of amplifiers is allowed to vary it may affect the optimum point significantly.

Choosing a value for the monitoring and management power consumption presents a challenge as estimates varies widely between different sources. In [9] a value as high as 100 W is used for the total EDFA power consumption and [16] uses a value of 55 W for the monitoring and management power consumption. In [48, 49] the whole amplifier power consumption is estimated to be between 30 W and 60 W. In contrast to these values, Desbruslais et al. [47] use a value of 10% of the total amplifier power consumption, which would correspond to sub-Watt values for a typical amplifier.

3.4 System optimization

By combining power consumption and noise models, the relation between system performance and amplifier power consumption can be studied. Several studies of this has been published, and depending on the exact system model used the results may differ. In this section the different approaches and results are compared and discussed.

3.4.1 EDFA

One of the simplest system models is to combine the added-power model with the standard OSNR model. In [9] this is done to estimate the theoretical lower limit on amplifier power consumption. In this model, the power consumption is directly proportional to the signal launch power, and fiber nonlinearities are neglected. If the required SNR is fixed, the power consumption becomes directly proportional to the noise power added in the line amplifiers. Thus, the power consumption grows exponentially with system length. Shorter spans lead to a slower build-up of ASE noise, and thus result in a lower power consumption. The span length that achieves the lowest power consumption is zero, which corresponds to ideal distributed amplification.

The situation changes if nonlinear effects are taken into account. Doran and Ellis [50] investigate the situation where performance is determined by the GN-model and optical output power is used as a power consumption measure. Then, the power consumption can be analyzed analytically, and an optimum point that minimizes the power consumption can be found. Depending on how the signal launch power is chosen the optimum point will be different. Either, the system can be operated at the nonlinear threshold (in this thesis Eq. (2.2)), or the signal power can be chosen to always achieve a certain OSNR. In the first case, where the system is operated at the nonlinear threshold the span length that gives the minimum power consumption is $L = 3/\alpha$, where α is the fiber attenuation in m^{-1} . This corresponds to a loss of 13 dB, which for a typical SMF is 65 km. In the second case, which is a more global optimum, the span length is shorter than in the first case. The minimum points exists due to the following trade-off: For span lengths longer than the optimum, the power consumption increases since the increased ASE requires the signal launch power to be increased. For span lengths lower than the optimum, the power consumption increases since more EDFAs are needed.

In [Paper A] we investigate the system level power consumption by combining the added-power model (including the monitoring and management power consumption) with the GN-model. In a multi-span system, if the system is assumed to be

operated at the optimal signal launch power the power consumption can be studied as a function of the OSNR by varying the number of spans, and thus the span length. When the number of spans is increased, the OSNR is increased. Since the amount of ASE then is lower, the optimal signal launch power is also lower. This leads to the pump power consumption being lower. However, since the number of amplifiers is increased the total monitoring and management power consumption is increased. This means that for a fixed system length, the OSNR that gives the lowest amplifier power consumption will be a trade-off between pump power consumption and monitoring and management power consumption.

3.4.2 Hybrid Raman amplification

Due to its low power conversion efficiency, distributed Raman amplification generally requires significantly higher pump power to provide the same gain as an EDFA. However, its beneficial noise properties can lead to power savings in other parts of the systems that outweigh the increased pump power consumption [Paper A]. These situations are either if the monitoring and management power consumption is high or if the OSNR requirement is high, such as for high-order modulation formats.

Chapter 4

Digital signal processing

One of the key factors to the success of coherent detection is that the access to the full optical field enables the use of digital signal processing (DSP) to be used to efficiently compensate linear transmission impairments. In addition, DSP enables the use of a free-running local oscillator (LO), since frequency offset and phase-noise can be tracked digitally, which avoids the use of complex analog control loops. However, the digital circuits performing the processing is one of the major power consumers in a coherent receiver [16].

In this chapter we cover the basics of digital signal processing in coherent fiber-optical communication systems, along with an overview of implementation and power consumption issues.

4.1 Overview of DSP for coherent systems

Coherent optical communication relies on digital signal processing in several steps. In Fig. 4.1, a schematic of a typical DSP-chain is shown. Signal processing is needed both to compensate for impairments caused by non-ideal components and fiber-related transmission impairments.

4.1.1 Optical front-end correction

Optical front-end correction compensates for the impairments introduced by the photodetectors and the optical hybrid. In particular, normalization compensates for unequal responsivities of the photodetectors and orthogonalization compensates for imperfect 90° phase-shift in the optical hybrid. The most common orthogonalization al-

are synchronous standards where clocks are synchronized over the system, while Ethernet allows the clocks to differ, and thus requires clock frequency recovery.

Several algorithms exist for performing timing recovery separately [21], but it can also be performed by adaptive finite impulse response (FIR) filters [55] like those needed for compensation of polarization-mode dispersion (PMD), discussed in next section.

4.1.4 Adaptive equalization

Adaptive equalization is needed to compensate for time-varying effects. In a fiber-optic systems the most important time-varying effects are polarization changes and PMD. Since polarization rotations causes linear mixing of the two polarizations, polarization demultiplexing is performed with a 2×2 multiple-input multiple-output (MIMO) equalizer. For this, only one filter tap is needed. However, since PMD introduces frequency dependent cross-talk between the polarizations, more taps are needed.

In addition to the time-varying effects, due to the adaptivity of the filter, the taps will adjust to compensate also static linear impairments remaining on the signal. This includes any CD not compensated for by the static CD equalizer and filtering characteristics in the signal paths, such as digital-to-analog converters (DACs), modulator, photodetectors and analog-to-digital converters (ADCs). The filter will also converge to match the signal spectrum, acting as a matched filter providing optimal noise filtering. If the error function used in the tap updating is sensitive to phase errors, slow phase drift can also be tracked. It is also common to perform downsampling in the adaptive equalizer in which case it will act as a timing recovery stage.

For QPSK the constant-modulus algorithm (CMA) [56, 57] is commonly used for tap update [21], relying on the constant power of the QPSK symbols. While it still works for higher order modulation formats, the tap updates become noisy which leads to poor performance [21]. The CMA can be modified for higher order modulation formats to include several power levels, known as radius-directed equalization (RDE) or the multi-modulus algorithm (MMA) [58, 59, 60, 61]. However for modulation formats with many radius levels such as 64QAM, this performs poorly. Another option is to use decision-directed update, where the error is the distance to the closest constellation point [58, 61]. This has the added advantage of being sensitive to phase, which means that the equalizer can track slow phase drift. However, this means that the error calculation needs to be done after the carrier recovery stage, which then ends up inside of the equalizer update loop.

4.1.5 Carrier recovery

Carrier recovery is performed in at least two stages. The first coarse stage estimates the bulk of the frequency offset between the carrier and the LO laser. This is typically done by finding peaks in the spectrum of the detected signal. After the coarse carrier recovery, in addition to some remaining small frequency offset also any phase drift due to laser phase noise needs to be recovered. Carrier recovery is described in detail in Chapter 5.

4.2 Implementation and power-consumption aspects

Due to the high throughput requirements, DSP for optical communication is generally implemented as application specific integrated circuits (ASICs). Implementation of real-time DSP presents a number of challenges.

Parallelization

As the typical clock frequency of an ASIC is below 1 GHz, it is not possible to process optical signals in serial manner. Instead, parallelization is used, which means that the signal and subsequently all processing units are divided into several parallel data streams and processing blocks. For many DSP functions this can be readily done without impacting the performance, but it might limit the tracking speed of fast time-varying impairments such as phase drift.

Quantization

Floating point arithmetics leads to a too high circuit complexity to be implemented in optical DSP. Therefore, computations are performed using fixed-point arithmetics which requires quantization of the signal. Since complexity and power dissipation increases with the number of quantization levels, it is desirable to use as few quantization levels as possible without giving rise to a penalty due to quantization noise. Generally, higher order modulation formats require more quantization levels.

4.2.1 Power consumption

The power consumption of ASICs depends on the logic functions they perform and the clock-frequency of which the circuit runs in a complex manner. This is because fundamentally the power consumption is determined by the physical layout of the circuit on a transistor level, where also internal interconnecting wires may play a significant role. In addition, the power consumption depends on the the signal being

processed [62, Ch. 5]. This makes it hard to estimate power consumption directly from any given algorithm. As of today, the most reliable way of estimating the power consumption of a DSP algorithm is to design an ASIC—including physical layout—and simulate it with realistic input signals. Since this requires considerable ASIC-design skills and also then a significant workload, analysis of algorithms tend to be based on computational complexity, where the number of operations required for an algorithm is compared. While this is often the only feasible option, the results can only give a rough indication of actual power consumption [63].

An alternative is scaling values from an ASIC implementation with some design parameter, as in [Paper B] where we used the equalizer design in [63] and rescaled with the number of taps. This was possible since the equalizer considered in [Paper B] have a similar structure to the one in [63].

4.2.2 Relative power consumption of the steps in DSP for optical communications

In [16], Pillai et al. analyze DSP power consumption by basing their estimates on counting operations, while Crivelli et al. [64] and Morero et al. [23] base their values on actual power consumption of commercial chips. Although the individual estimates differ, the overall picture is similar. All three sources find that compensation of chromatic dispersion is the major power consumer followed by the adaptive equalizer responsible for PMD-compensation. While carrier recovery is found to be on third place, it is still has a significantly lower power consumption than the top two. Both [16] and [23] compare QPSK to 16QAM and find that the higher order format achieves an equivalent [16] or lower [23] power consumption per bit.

In a long-haul link, where high amounts of CD and PMD needs to be compensated for, the DSP power consumption is comparable to that of optical components such as lasers, modulators and optical amplifiers [16]. However, in the short-reach limit where no length dependent signal impairments are present, the DSP functions consume only a small part of the power [Paper B].

Chapter 5

Advanced methods for carrier recovery

In early coherent systems, the local oscillator (LO) was synchronized to the frequency of the transmitter laser in an analog fashion [65] but in modern systems the LO tend to be free-running and carrier recovery performed digitally, which now can be considered the standard method. However, on a third place after chromatic and polarization mode dispersion compensation, carrier recovery is one of the major parts of the power consumption of the digital signal processing (DSP) [16, 23, 64]. Combined with the additional phase-noise sensitivity of higher order modulation formats that puts further pressure on the phase-tracking, this makes optical methods for relieving the digital carrier-recovery attractive.

This chapter covers the principles of digital carrier recovery in more detail, and presents ways of utilizing optical methods together with DSP to achieve a more efficient carrier recovery.

5.1 Carrier frequency offset and phase-drift

With a free-running LO, the different center frequencies of the transmitter and LO lasers will cause the detected signal to have remaining frequency offset. In addition, the lasers have a finite linewidth, which means that their phases will fluctuate. Furthermore, nonlinear propagation effects can cause phase distortions on the signal. Laser phase noise is commonly modelled as a Wiener process

$$\theta_k = \theta_{k-1} + \Delta_k, \quad (5.1)$$

where θ_k is the phase of the k -th sample, and the Δ_k is a real random Gaussian variable with zero mean and variance

$$\sigma_\theta^2 = 2\pi\Delta f T_s. \quad (5.2)$$

Here Δf is the combined laser linewidth of the transmitter and LO laser and T_s is the symbol period.

5.2 Pilot-tone based carrier-recovery

Digital carrier-recovery can be significantly simplified or completely removed if the unmodulated carrier is transmitted as a pilot-tone. Pilot-tones can be inserted as an electrical subcarrier [66] or optically in various ways. For example, the signal can be polarization multiplexed with an unmodulated carrier, which works as a pilot-tone [67, 68, 69]. At the receiver, the polarization is aligned and the pilot-tone is used instead of an LO. This is known as self-homodyne detection. Alternatively, the signal and pilot-tone can be detected with a Stokes polarimeter [70, 71] which enables digital polarization tracking. Pilot-tone based schemes can tolerate very high laser linewidths and also cancel nonlinear phase distortions [72]. In addition, digital carrier-recovery can be omitted. However, since the pilot-tone is transmitted on one of the polarizations, spectral efficiency is reduced by half. In addition, ASE noise is added to the pilot-tone during transmission, which leads to an OSNR penalty [73]. This effect can be partly reduced by filtering of the pilot-tone. Self-homodyne detection can also be realized in multi-core fibers (MCF), where the pilot-tone is transmitted on one core [74]. Since the pilot-tone can be shared between all the cores, the reduction in spectral efficiency is not as prominent as when the pilot-tone is polarization multiplexed with the signal.

The pilot-tone can also be detected and the self-homodyne mixing performed digitally. In the polarization-multiplexed case this is known as digital self-homodyne detection [75] and in the MCF case shared-carrier reception [76]. The advantages of detecting the pilot-tone digitally is that polarization tracking and pilot-tone filtering can be performed digitally. In [Paper B] digital self-homodyne detection was used.

5.3 Digital carrier-recovery methods

DSP-based carrier recovery is commonly divided into steps, where a first coarse carrier-recovery compensates for the main parts of the frequency offset. Once this offset has been removed, significant amounts of phase-drift still remain on the signal, which is estimated and compensated for by the phase-tracking.

5.3.1 Frequency offset estimation

The frequency offset can be estimated by finding the peak of the spectrum of the 4th power of the signal [21], which relies on the same principle to remove the modulation as the Viterbi-Viterbi algorithm [77] described later. Although the modulation cannot be completely removed for higher order QAM formats, this method is still useful, albeit with a lower accuracy.

5.3.2 Feedback-based phase-tracking

Early coherent receivers were based on analog phase-locked loops for carrier recovery [65], where an error signal calculated from the signal is used to tune the frequency of the LO laser. The feedback principle can also be used in DSP, for example as in the decision-directed (DD) phase estimator in [78]. In this algorithm, the signal is derotated with the phase angle estimated from a previous symbol, with some feedback delay. This algorithm can achieve high tracking speeds if the feedback delay is low. However, the effect of the parallelization necessary in an ASIC implementation is to increase the delay, so the tracking speed is severely limited in a hardware implementation [79]. Still, feedback methods can be used if they are combined with faster algorithms [64].

5.3.3 The Viterbi-Viterbi algorithm

For QPSK, the Viterbi-Viterbi algorithm [77] is commonly used. Single amplitude M -PSK modulation formats has the property that if the M -th power of the symbols is taken, all symbols are mapped to the same point. This has the effect of removing the modulation, and can be used to estimate the phase drift [21]. For QPSK, $M = 4$, and the estimated phase is

$$\phi_k = \frac{1}{4} \sum_{|n| < L/2} w_n \arg [Z_{k+n}^4], \quad (5.3)$$

Here Z_k is the k -th symbol. To minimize the effect of additive Gaussian noise, estimates of a block of consecutive symbols are weighed together with the weighing function w_n . In the simplest case, all $w_n = 1$ which is just a sliding average.

Since higher order QAM formats do not fulfill the single-amplitude condition, the Viterbi-Viterbi algorithm does not work well. However, this can be overcome by partitioning the symbols into groups with constant amplitude and applying the Viterbi-Viterbi algorithm to these [80].

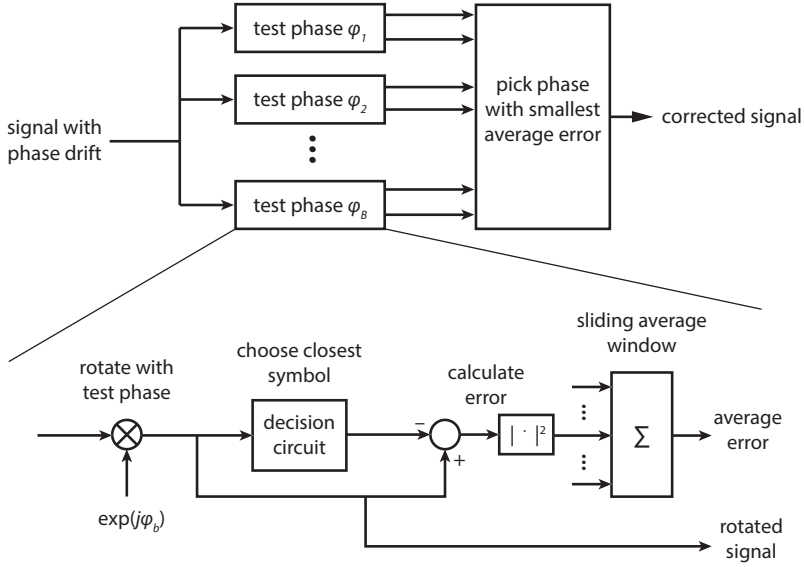


Figure 5.1: Schematic of the BPS algorithm.

5.3.4 Blind phase search

The blind phase-search (BPS) algorithm was first proposed in [81] and introduced to fiber optical communication in [79]. The working principle is as follows. The received signal Z_k , sampled at symbol rate, is first rotated with B test phase angles simultaneously

$$\phi_b = \frac{b}{B} \cdot \frac{\pi}{2}, \quad b = 0, 1, \dots, B-1 \quad (5.4)$$

after which the distance to the closest constellation symbol is calculated for each test angle as

$$|d_{k,b}|^2 = |Z_k e^{-j\phi_b} - \hat{X}_{k,b}|^2. \quad (5.5)$$

To reduce the impact of additive noise, the distances are then summed for L consecutive symbols

$$e_{k,b} = \sum_{|n| < L/2} |d_{k-n,b}|^2, \quad (5.6)$$

and the estimated phase angle is chosen as the one that minimizes $e_{k,b}$. The length of the summing window L is chosen as a trade-off between additive noise tolerance and

phase-noise tolerance, where a higher tolerance to phase-noise is achieved for large values of L . The strength of the BPS algorithm is that it can achieve high tracking speeds even if it is parallelized. This is due to the fact that it is inherently parallel as all test angles are calculated simultaneously. However, even if it was introduced to fiber optics as being "hardware efficient" the computational load scales linearly with the number of test angles. Thus for higher order QAM formats such as 64QAM that require a high angular resolution, the hardware requirements of BPS might become prohibitively high [82].

To address this and other issues, several variations and extensions of the BPS algorithm have been proposed. The phase estimation can be divided into several stages [82], where a first stage providing a rough estimate is followed by a more precise second stage. The different stages can use different algorithms [82, 83] or both be of the BPS type [84, 85]. One approach relies on the fact that $e_{k,b}$ can be approximated as a quadratic function of the test angle ϕ_b [86]. By applying a correction angle $\phi_{k,c}$ calculated using a quadratic approximation of $e_{k,b}$, the number of test angles needed can be significantly reduced. The final estimated phase angle is then

$$\phi_k = \phi_{k,b} + \phi_{k,c} = \phi_{k,b} + \frac{\Delta\phi}{2} \cdot \frac{e_{k,b-1} - e_{k,b+1}}{e_{k,b-1} + e_{k,b+1}}, \quad (5.7)$$

where $\Delta\phi = \pi/(2B)$ is the spacing between the test phase angles. The phase tracking in [Paper C] was based on this method.

5.3.5 Phase unwrapping and cycle slips

All the blind phase estimation algorithms discussed have a limited estimation range, and thus require phase unwrapping. The Viterbi-Viterbi algorithm produces phase values between $-\pi/M$ and π/M and the DD feedback algorithm is constrained to output values between $-\pi$ and π [78]. The output range of the BPS algorithm depends on the symmetries of the modulation format used. For square QAM, the the output of BPS is constrained to a $\pi/2$ range. When the phase reaches the end of the estimation range, the estimated phase will wrap around and make a jump to the other end of the range. This jump can be detected, and the phase unwrapped by adding an integer multiple of the estimation range. However, if the phase jump was present in the actual phase, phase unwrapping will cause a persistent phase error of a multiple of $\pi/2$. This is known as a cycle slip, which leads to catastrophic failures. To mitigate the effect of cycle slips, differential encoding can be used. Then, for square QAM, the two bits that determine the quadrant is differentially encoded similar to differentially encoded QPSK [78, 79]. However, this leads to an SNR penalty. Differential encoding is studied in detail in [87].

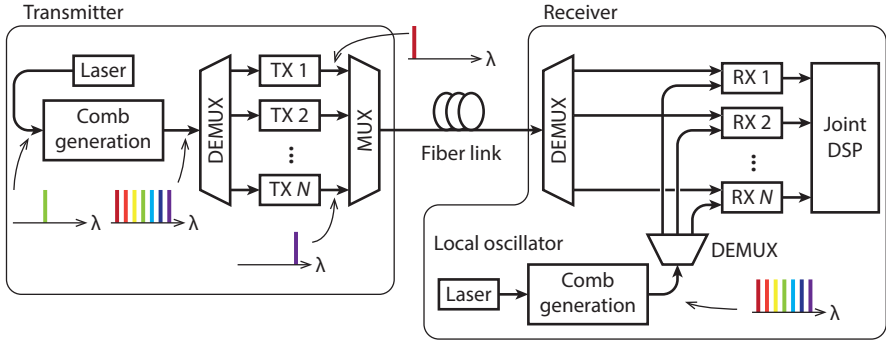


Figure 5.2: Schematic of a frequency-comb based system with joint DSP.

5.4 Joint carrier-recovery

If several channels share similar phase-drift, this shared information can be utilized to make the phase-tracking more efficient. This is in fact possible already in polarization-multiplexed systems [88] as long as the polarizations share the same transmitter and LO laser, which is typically the case. Spatial-division multiplexing (SDM) and frequency-comb based superchannels enables to extend this concept to a much larger number of channels, and can possibly give large performance gains or complexity savings.

5.4.1 Phase-locked multichannel systems

Frequency-comb based systems

One of the main characteristics of optical frequency combs is that the lines have a high phase coherence [89]. In a multi-wavelength system where frequency combs are used as carrier and LO sources, illustrated in Fig. 5.2, the phase drift on the detected signals will be highly correlated and the phase-tracking can be performed jointly. This was proposed by Liu et al. [90]. Similar, but much less scalable, is joint processing of electrical subcarriers, as demonstrated in [91].

There exist many techniques to generate optical frequency combs [89], but particularly interesting for optical communication are electro-optic combs [89, 92] and microresonator combs [93]. While most of the phase-noise of the combs originates from the phase-noise of the seed laser, which will be shared between the comb lines, some additional phase-noise will be added by the comb generation process [94]. It is

not yet clear to what extent this will affect the possibilities of joint phase-recovery. If the transmitter and LO frequency combs are not synchronized, the frequency offset will differ between the channels, and generally cannot be estimated jointly. However, if electro-optic combs are used, the difference in frequency offset is due to differences in frequency of the RF-clocks driving the combs. Since the frequency of radio-frequency (RF) clocks typically is stable over time, the frequency difference can be tracked very slowly. In [Paper C], where we demonstrated joint carrier-recovery using two free-running electro-optic combs, we observed sub-kHz stability over several days of measurements. In addition, we observed some small phase-drift differences between the channels that we tracked with a slow decision-directed feedback phase-tracker.

Spatial division multiplexed systems

In SDM systems, the spatial modes typically share the same lasers, and joint phase-tracking has been demonstrated both for multicore [95] and multimode [96] fibers. Here, joint processing is performed on the same wavelength on the different spatial modes, in contrast to the comb-based systems. Thus, there is no comb-generation contributing to different frequency offsets and frequency offset compensation can be performed jointly with no additional information. However, even though references [95] and [96] does not report using any additional slow individual phase tracking, small skew fluctuations have been measured between the cores of MCF [97, 98], and it is likely that some individual phase-tracking would be needed for long-term stability also in SDM systems.

5.4.2 Algorithms for joint phase-tracking

The term joint phase-tracking is often used loosely to describe all phase-tracking schemes that process several channels together, but includes two main categories that have quite different principles and benefits. The first scheme is joint phase *estimation*, where the phase information from all channels is used to estimate their common phase drift. Joint estimation was used in [91]. Opposed to joint-estimation is what is best described as *master-slave* schemes, where the phase drift is estimated from one channel—the master channel—and then used to compensate the phase drift of all the channels, which was used in [95, 96] and [Paper C]. In joint-estimation schemes the shared information is utilized to provide a better phase estimate, for example by replacing time-averaging with averaging over channels, which improves the tracking speed. In contrast, master-slave schemes do not strive to improve the performance but instead to reduce the overall hardware effort. These schemes are illustrated in

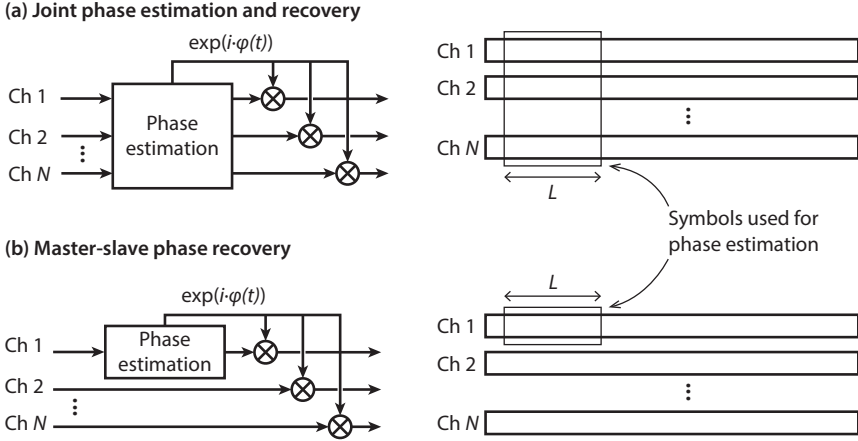


Figure 5.3: Comparison of the principle of (a) Joint phase estimation (b) Master-slave phase recovery.

Fig. 5.3. In addition, any constant or time varying phase difference between the channels needs to be compensated for individually on the channels.

Joint estimation

The blind phase estimation schemes presented earlier can relatively easily be extended to several channels by including single-symbol estimates from several channels in the time-averaging filters. This is described for the Viterbi-Viterbi algorithm in [90]. The inclusion of additional symbols in the averaging increase the SNR-tolerance, and the the filter length L can be reduced while still maintaining the same tolerance to Gaussian noise. This way the tracking speed can be increased [91]. However, it should be noted that a performance increase can only be expected if the system otherwise is limited by phase-noise. Any individual tracking of inter-channel phase differences has to be performed before the main joint-estimation stage so that the differences does not impact the joint estimation. If the phase difference is very slowly varying, it can be found by periodically running single-channel phase estimation separately on the channels, but also feedback methods that perform individual estimation after the main phase-drift compensation may be useful.

Although the phase noise tolerance of joint estimation schemes is higher, the computational complexity is not significantly reduced even if the averaging length L is reduced. This is because the averaging operation is not the most resource inten-

sive, and single-symbol phase estimation will nevertheless need to be performed. In addition, the offset tracking adds some complexity.

Master-slave phase recovery

Master-slave phase recovery is straightforward. Phase estimation is performed as in the single-channel case on the master channel, and the estimated phase is used for the slave channels. For master-slave schemes the inter-channel phase difference is preferably estimated after the phase-drift compensation since it is easier when the main phase drift has been compensated for. As long as any inter-channel phase differences are compensated or negligible, performance will be the same as for individual carrier recovery.

How much reduction of computational complexity is possible to achieve will depend on the algorithm used and more specifically the relation between the complexity of the estimation and the compensation parts.

5.4.3 Effects of optical delay

Different optical delay of the jointly processed channels is a limiting factor for joint phase-compensation. This is not easily compensated for electronically since the phase drift on the detected signal is a sum of the phase-drift from both the transmitter and LO lasers. Since only the phase-drift of the transmitter laser will be delayed, the phase-drift of the detected signals will not just be delayed versions of one another. Sources of delay can be path length differences in optical components, but also chromatic dispersion in comb-based systems and differential group delay in multi-mode systems. This will effectively limit the transmission distance for which joint processing is possible.

Chapter 6

Future outlook

Optical frequency comb based systems

There are many interesting question remaining relating to the use of optical frequency combs in multi-wavelength transceivers.

- The impact of limited comb coherence on the joint carrier-recovery schemes needs to be further investigated. We have shown in [Paper C] that electro-optical combs have a difference that can be compensated for, but to get the full picture, the phase relations of the combs lines should be measured directly. In addition, this should be combined with modelling efforts, to enable the design of possibly more efficient algorithms.
- Joint carrier-recovery with more compact comb sources such as microresonator combs remains to be demonstrated, and as for electro-optical combs it is not yet fully known how the phase relations between lines from these comb sources affect joint carrier-recovery schemes.
- Transmission effects on the phase-relations between the channels have not been investigated. Chromatic dispersion will create a timing offset between the channels which will limit the transmission reach, and nonlinear effects will affect the wavelength channels differently.
- A full-system approach needs to be taken to determine how the use of optical frequency combs will affect the overall power consumption. Even if the DSP power consumption can be decreased, the comb generation process is associated with some power consumption which needs to be accounted for. Optical

frequency combs can also lead to power savings since they take the place of individual transmitter and LO lasers.

- A synchronized multi-channel receiver also enables joint estimation of other correlated effects, such as polarization rotations and PMD. In addition, impairments such as interchannel interference can also be compensated. The possibilities of complexity reductions or performance boost utilizing this should be investigated.

Power consumption of broadband Raman amplification

In [Paper A] we investigated the trade-offs related to the power consumption when Raman amplification is used to increase the OSNR of the signal. However, Raman amplification can also be used to enable amplification over a wider bandwidth than in EDFA-based systems. This can be used to increase the capacity of a single fiber, which could be more energy efficient than adding an extra fiber.

DSP power consumption modelling

There are many interesting research questions involving power consumption trade-offs between DSP and other parts of the system. The work on these issues are currently limited by the lack of accurate DSP power consumption models that do not involve designing a full ASIC. Developing such models would enable more accurate predictions of the overall power consumption.

Chapter 7

Summary of papers

Paper A

Power Consumption Analysis of Hybrid EDFA/Raman Amplifiers in Long-Haul Transmission Systems,

Journal of Lightwave Technology, vol. 35, no. 11, pp. 2132–2142, 2017.

Here we analyze the power consumption of optical amplifiers and trade-offs between this and signal quality in terms of OSNR. We study both EDFAs and backwards pumped Raman amplification, and include also the power consumption of monitoring and management electronics. We find that the value of power consumption of the monitoring and management electronics significantly affects which system configuration gives the lowest power consumption.

We also study the impact modulation format and choice of FEC scheme has on the energy consumption per bit. We find that 16QAM is more energy efficient than QPSK, and that there are cases when it might be more energy efficient to increase the the signal quality by shortening the spans instead of using a powerful FEC scheme.

Paper B

Power Consumption of a Minimal-DSP Coherent Link with a Polarization Multiplexed Pilot-Tone,

European Conference on Optical Communication (ECOC), Düsseldorf, Germany, paper Th.2.P2.SC5.58, 2016.

As the demand for bandwidth increase also for short systems, coherent technologies is become more attractive also for this kind of links. Then, as length dependent impairments no longer need to be compensated for in DSP, the power consumption trade-offs become different. In this paper, we study the power consumption of a link with minimal DSP aided by a polarization-multiplexed pilot-tone. The DSP power consumption is estimated by scaling values from a similar structure ASIC implementation. We find that the system power consumption is dominated by the optical components.

Paper C

Joint Carrier Recovery for DSP Complexity Reduction in Frequency Comb-Based Superchannel Transceivers,

European Conference on Optical Communication (ECOC), Gothenburg, Sweden, paper Th.1.D.3, 2017.

In this paper we investigate the possibilities of performing joint carrier-recovery in frequency comb-based links. We demonstrate master-slave carrier-recovery on 10 GBaud PM-64QAM signals with phase-locked wavelength carriers with negligible penalty up to a frequency spacing of ± 275 GHz. We find a small remaining phase variation on the slave channels whose standard deviation grows linearly with the frequency spacing to the master channel. The remaining phase variation is compensated for with a slow, low complexity feedback phase-tracker.

Bibliography

- [1] “ICT facts and figures 2017,” International Telecommunication Union.
- [2] K. Kao and G. Hockham, “Dielectric-fibre surface waveguides for optical frequencies,” *Proceedings of the Institution of Electrical Engineers*, vol. 113, no. 7, pp. 1151–1158, 1966.
- [3] T. H. Maiman, “Stimulated Optical Radiation in Ruby,” *Nature*, vol. 187, no. 4736, pp. 493–494, 1960.
- [4] R. Mears, L. Reekie, I. Jauncey, and D. Payne, “Low-noise erbium-doped fibre amplifier operating at $1.54\mu\text{m}$,” *Electronics Letters*, vol. 23, no. 19, pp. 1026–1028, 1987.
- [5] H. Sun, K.-T. Wu, and K. Roberts, “Real-time measurements of a 40 Gb/s coherent system,” *Optics Express*, vol. 16, no. 2, pp. 873–879, 2008.
- [6] C. E. Shannon, “A Mathematical Theory of Communication,” *Bell System Technical Journal*, vol. 27, no. 3, pp. 379–423, 1948.
- [7] M. J. Golay, “Notes on digital coding,” *Proceedings of the Institute of Radio Engineers*, vol. 37, no. 6, pp. 657–657, 1949.
- [8] R. W. Hamming, “Error Detecting and Error Correcting Codes,” *Bell System Technical Journal*, vol. 29, no. 2, pp. 147–160, 1950.
- [9] R. S. Tucker, “Green optical communications—Part I: Energy limitations in transport,” *IEEE Journal of Selected Topics in Quantum Electronics*, vol. 17, no. 2, pp. 245–260, 2011.
- [10] D. C. Kilper, G. Atkinson, S. K. Korotky, S. Goyal, P. Vetter, D. Suvakovic, and O. Blume, “Power Trends in Communication Networks,” *IEEE Journal of Selected Topics in Quantum Electronics*, vol. 17, no. 2, pp. 275–284, 2011.

Bibliography

- [11] “Climate Change 2013: The Physical Science Basis,” Intergovernmental Panel on Climate Change (IPCC).
- [12] J. C. Geyer, C. Rasmussen, B. Shah, T. Nielsen, and M. Givehchi, “Power efficient coherent transceivers,” in *European Conference on Optical Communication (ECOC)*, 2016.
- [13] “HIS Infonetics 100G+ Coherent Optical Equipment Ports Manual Market Share Size and Forecasts,” 2015. [Online]. Available: <http://news.ihsmarket.com/press-release/technology/ihs-forecasts-huge-growth-100-gigabit-optical-ports-operators-increase-netw>
- [14] X. Zhou and H. Liu, “Pluggable DWDM: Considerations For Campus and Metro DCI Applications,” in *European Conference on Optical Communication (ECOC)*, 2016. [Online]. Available: <https://static.googleusercontent.com/media/research.google.com/en//pubs/archive/45713.pdf>
- [15] “Neophotonics ITLA,” <https://www.neophotonics.com/product/itla/>, accessed: 2017-07-29.
- [16] B. S. G. Pillai, B. Sedighi, K. Guan, N. P. Anthapadmanabhan, W. Shieh, K. J. Hinton, and R. S. Tucker, “End-to-end energy modeling and analysis of long-haul coherent transmission systems,” *Journal of Lightwave Technology*, vol. 32, no. 18, pp. 3093–3111, 2014.
- [17] K.-P. Ho, *Phase-modulated optical communication systems*. Springer Science & Business Media, 2005.
- [18] S. S. Azadeh, F. Merget, S. Romero-García, A. Moscoso-Mártir, N. von den Driesch, J. Müller, S. Mantl, D. Buca, and J. Witzens, “Low $V\pi$ Silicon photonics modulators with highly linear epitaxially grown phase shifters,” *Optics Express*, vol. 23, no. 18, pp. 23 526–23 550, 2015.
- [19] R. Nagarajan, M. Kato, J. Pleumeekers, P. Evans, S. Corzine, S. Hurtt, A. Dentai, S. Murthy, M. Missey, R. Muthiah, R. A. Salvatore, C. Joyner, R. Schneider, M. Ziari, F. Kish, and D. Welch, “InP Photonic Integrated Circuits,” *IEEE Journal of Selected Topics in Quantum Electronics*, vol. 16, no. 5, pp. 1113–1125, 2010.
- [20] M. Seimetz and C.-M. Weinert, “Options, feasibility, and availability of 2x4 90 deg hybrids for coherent optical systems,” *Journal of Lightwave Technology*, vol. 24, no. 3, pp. 1317–1322, 2006.

-
- [21] S. J. Savory, "Digital Coherent Optical Receivers: Algorithms and Subsystems," *IEEE Journal of Selected Topics in Quantum Electronics*, vol. 16, no. 5, pp. 1164–1179, 2010.
- [22] B. P. Ginsburg and A. P. Chandrakasan, "Dual Time-Interleaved Successive Approximation Register ADCs for an Ultra-Wideband Receiver," *IEEE Journal of Solid-State Circuits*, vol. 42, no. 2, pp. 247–257, 2007.
- [23] D. A. Morero, M. A. Castrillon, A. Aguirre, M. R. Hueda, and O. E. Agazzi, "Design Tradeoffs and Challenges in Practical Coherent Optical Transceiver Implementations," *Journal of Lightwave Technology*, vol. 34, no. 1, pp. 121–136, 2016.
- [24] A. Alvarado, E. Agrell, D. Lavery, R. Maher, and P. Bayvel, "Replacing the Soft-Decision FEC Limit Paradigm in the Design of Optical Communication Systems," *Journal of Lightwave Technology*, vol. 34, no. 2, pp. 707–721, 2016.
- [25] B. S. G. Pillai, B. Sedighi, W. Shieh, and R. S. Tucker, "Chromatic Dispersion Compensation – An Energy Consumption Perspective," in *Optical Fiber Communication Conference (OFC)*, 2012, p. OM3A.8.
- [26] E. Tipsuwannakul, J. Li, T. A. Eriksson, L. Egnell, F. Sjöström, J. Pejnefors, P. A. Andrekson, and M. Karlsson, "Influence of Fiber-Bragg Grating-Induced Group-Delay Ripple in High-Speed Transmission Systems," *Journal of Optical Communications and Networking*, vol. 4, no. 6, pp. 514–521, 2012.
- [27] E. Ip and J. M. Kahn, "Compensation of Dispersion and Nonlinear Impairments Using Digital Backpropagation," *Journal of Lightwave Technology*, vol. 26, no. 20, pp. 3416–3425, 2008.
- [28] R. Dar and P. J. Winzer, "On the Limits of Digital Back-Propagation in Fully Loaded WDM Systems," *IEEE Photonics Technology Letters*, vol. 28, no. 11, pp. 1253–1256, 2016.
- [29] C. Fougstedt, M. Mazur, L. Svensson, H. Eliasson, M. Karlsson, and P. Larsson-Edefors, "Time-Domain Digital Back Propagation: Algorithm and Finite-Precision Implementation Aspects," in *Optical Fiber Communication Conference (OFC)*, 2017, p. W1G.4.
- [30] V. Parahyba, J. Reis, S. Ranzini, E. Schneider, E. Rosa, F. Simões, J. Diniz, L. Carvalho, E. Filho, J. Oliveira, and J. Oliveira, "Performance against implementation of digital backpropagation for high-speed coherent optical systems," *Electronics Letters*, vol. 51, no. 14, pp. 1094–1096, 2015.

- [31] P. Poggiolini, “The GN Model of Non-Linear Propagation in Uncompensated Coherent Optical Systems,” *Journal of Lightwave Technology*, vol. 30, no. 24, pp. 3857–3879, 2012.
- [32] P. Johannisson and M. Karlsson, “Perturbation Analysis of Nonlinear Propagation in a Strongly Dispersive Optical Communication System,” *Journal of Lightwave Technology*, vol. 31, no. 8, pp. 1273–1282, 2013.
- [33] E. Agrell, A. Alvarado, G. Durisi, and M. Karlsson, “Capacity of a nonlinear optical channel with finite memory,” *Journal of Lightwave Technology*, vol. 32, no. 16, pp. 2862–2876, 2014.
- [34] A. A. M. Saleh, R. M. Jopson, J. D. Evankow, and J. Aspell, “Modeling of gain in erbium-doped fiber amplifiers,” *IEEE Photonics Technology Letters*, vol. 2, no. 10, pp. 714–717, 1990.
- [35] R. M. Jopson and A. A. Saleh, “Modeling of gain and noise in erbium-doped fiber amplifiers,” in *Proceedings of the SPIE*, vol. 1581, no. 2, 1992, pp. 114–119.
- [36] P. C. Becker, N. A. Olsson, and J. R. Simpson, *Erbium-doped fiber amplifiers: fundamentals and technology*. San Diego: Academic Press, 1999.
- [37] H. Kogelnik and A. Yariv, “Considerations of Noise and Schemes for Its Reduction in Laser Amplifiers,” *Proceedings of the IEEE*, vol. 52, no. 2, pp. 165–172, 1964.
- [38] R. H. Stolen, W. J. Tomlinson, H. A. Haus, and J. P. Gordon, “Raman response function of silica-core fibers,” *Journal of the Optical Society of America B*, vol. 6, no. 6, pp. 1159–1166, 1989.
- [39] V. Curri and A. Carena, “Merit of Raman pumping in uniform and uncompensated links Supporting NyWDM transmission,” *Journal of Lightwave Technology*, vol. 34, no. 2, pp. 554–565, 2016.
- [40] C. Headley and G. P. Agrawal, *Raman amplification in fiber optical communication systems*. Elsevier Academic Press, 2005.
- [41] V. Curri, A. Carena, P. Poggiolini, G. Bosco, and F. Forghieri, “Extension and validation of the GN model for non-linear interference to uncompensated links using Raman amplification,” *Optics Express*, vol. 21, no. 3, pp. 3308–3317, 2013.

-
- [42] W. S. Pelouch, "Raman amplification: An enabling technology for long-haul coherent transmission systems," *Journal of Lightwave Technology*, vol. 34, no. 1, pp. 6–19, 2016.
- [43] D. Enescu and E. O. Virjoghe, "A review on thermoelectric cooling parameters and performance," *Renewable and Sustainable Energy Reviews*, vol. 38, pp. 903–916, 2014.
- [44] L. A. Johnson, *Application note: Controlling temperatures of diode lasers and detectors thermoelectrically*, Newport Corporation, Accessed: 2016-11-07. [Online]. Available: https://www.newport.com/medias/sys_master/images/images/hcc/hc7/8797049389086/AN01-Controlling-Temperatures-of-Laser-Diodes-Thermoelectrically.pdf
- [45] J. Yoshida, C. F. Hayamizu, H. Itoh, M. Miura, T. Sawamura, S. Irino, T. Takeuchi, T. Kimura, and N. Tsukiji, "2.8 FITs of Field Reliability of 1480nm/14xx-nm Pump Lasers," in *Optical Fiber Communication Conference (OFC)*, 2015, p. W2A.2.
- [46] "Finisar fixed gain EDFA," https://www.finisar.com/sites/default/files/downloads/finisar_amplifier_fixed_gain_edfa_product_brief.pdf, accessed: 2017-07-18.
- [47] S. Desbruslais, "Maximizing the capacity of ultra-long haul submarine systems," in *European Conference on Networks and Optical Communications (NOC)*, 2015.
- [48] W. Van Heddeghem, F. Idzikowski, W. Vereecken, D. Colle, M. Pickavet, and P. Demeester, "Power consumption modeling in optical multilayer networks," *Photonic Network Communications*, vol. 24, no. 2, pp. 86–102, 2012.
- [49] W. Van Heddeghem and F. Idzikowski, "Equipment power consumption in optical multilayer networks – source data," Tech. Rep., 2012. [Online]. Available: <http://powerlib.intec.ugent.be/>
- [50] N. J. Doran and A. D. Ellis, "Minimising total energy requirements in amplified links by optimising amplifier spacing," *Optics Express*, vol. 22, no. 16, pp. 19 810–19 817, 2014.
- [51] I. Fatadin, S. J. Savory, and D. Ives, "Compensation of Quadrature Imbalance in an Optical QPSK Coherent Receiver," *IEEE Photonics Technology Letters*, vol. 20, no. 20, pp. 1733–1735, 2008.

- [52] S. J. Savory, "Digital filters for coherent optical receivers," *Optics Express*, vol. 16, no. 2, pp. 804–817, 2008.
- [53] A. Sheikh, C. Fougstedt, A. Graell i Amat, P. Johannisson, P. Larsson-Edefors, and M. Karlsson, "Dispersion Compensation FIR Filter With Improved Robustness to Coefficient Quantization Errors," *Journal of Lightwave Technology*, vol. 34, no. 22, pp. 5110–5117, 2016.
- [54] C. Fougstedt, A. Sheikh, P. Johannisson, A. Graell i Amat, and P. Larsson-Edefors, "Power-Efficient Time-Domain Dispersion Compensation Using Optimized FIR Filter Implementation," in *Signal Processing in Photonic Communications (SPPCOM)*, 2015, p. SpT3D.3.
- [55] K. Kikuchi, "Clock recovering characteristics of adaptive finite-impulse-response filters in digital coherent optical receivers," *Optics Express*, vol. 19, no. 6, pp. 5611–5619, 2011.
- [56] D. Godard, "Self-Recovering Equalization and Carrier Tracking in Two-Dimensional Data Communication Systems," *IEEE Transactions on Communications*, vol. 28, no. 11, pp. 1867–1875, 1980.
- [57] K. Kikuchi, "Polarization-demultiplexing algorithm in the digital coherent receiver," in *Digest of the IEEE/LEOS Summer Topical Meetings*, no. 9, 2008, pp. 101–102.
- [58] W. Sethares, G. Rey, and C. Johnson, "Approaches to blind equalization of signals with multiple modulus," in *International Conference on Acoustics, Speech, and Signal Processing*, 1989, pp. 972–975.
- [59] M. Ready and R. Gooch, "Blind equalization based on radius directed adaptation," in *International Conference on Acoustics, Speech, and Signal Processing*, 1990, pp. 1699–1702.
- [60] J. Treichler, M. Larimore, and J. Harp, "Practical blind demodulators for high-order QAM signals," *Proceedings of the IEEE*, vol. 86, no. 10, pp. 1907–1926, 1998.
- [61] I. Fatadin, D. Ives, and S. Savory, "Blind Equalization and Carrier Phase Recovery in a 16-QAM Optical Coherent System," *Journal of Lightwave Technology*, vol. 27, no. 15, pp. 3042–3049, 2009.
- [62] N. H. E. Weste and D. M. Harris, *CMOS VLSI Design: A Circuits and Systems Perspective*. Addison-Wesley, 2011.

-
- [63] C. Fougstedt, P. Johannisson, L. Svensson, and P. Larsson-Edefors, "Dynamic Equalizer Power Dissipation Optimization," in *Optical Fiber Communication Conference (OFC)*, 2016, p. W4A.2.
- [64] D. E. Crivelli, M. R. Hueda, H. S. Carrer, M. del Barco, R. R. Lopez, P. Gianni, J. Finochietto, N. Swenson, P. Voois, and O. E. Agazzi, "Architecture of a Single-Chip 50 Gb/s DP-QPSK/BPSK Transceiver With Electronic Dispersion Compensation for Coherent Optical Channels," *IEEE Transactions on Circuits and Systems I: Regular Papers*, vol. 61, no. 4, pp. 1012–1025, 2014.
- [65] J. Barry and J. Kahn, "Carrier synchronization for homodyne and heterodyne detection of optical quadriphase-shift keying," *Journal of Lightwave Technology*, vol. 10, no. 12, pp. 1939–1951, 1992.
- [66] M. Morsy-Osman, Q. Zhuge, L. R. Chen, and D. V. Plant, "Feedforward carrier recovery via pilot-aided transmission for single-carrier systems with arbitrary M-QAM constellations," *Optics Express*, vol. 19, no. 24, pp. 24 331–24 343, 2011.
- [67] T. Miyazaki and F. Kubota, "PSK self-homodyne detection using a pilot carrier for multibit/symbol transmission with inverse-RZ signal," *IEEE Photonics Technology Letters*, vol. 17, no. 6, pp. 1334–1336, 2005.
- [68] T. Miyazaki, "Linewidth-tolerant QPSK homodyne transmission using a polarization-multiplexed pilot carrier," *IEEE Photonics Technology Letters*, vol. 18, no. 2, pp. 388–390, 2006.
- [69] M. Nakamura, Y. Kamio, and T. Miyazaki, "Linewidth-tolerant 10-Gbit/s 16-QAM transmission using a pilot-carrier based phase-noise cancelling technique," *Optics Express*, vol. 16, no. 14, pp. 10 611–10 616, 2008.
- [70] R. S. Luís, B. J. Puttnam, J. M. D. Mendinueta, Y. Awaji, and N. Wada, "Experimental demonstration of a polarization-insensitive self-homodyne detection receiver for optical access," in *European Conference on Optical Communication (ECOC)*, 2015.
- [71] D. Che, A. Li, and W. Shieh, "Blind polarization de-multiplexing for Stokes vector direct detection," in *European Conference on Optical Communication (ECOC)*, 2015.
- [72] P. Johannisson, M. Sjödin, M. Karlsson, E. Tipsuwannakul, and P. Andrekson, "Cancellation of nonlinear phase distortion in self-homodyne coherent systems," *IEEE Photonics Technology Letters*, vol. 22, no. 11, pp. 802–804, 2010.

- [73] M. Sjödin, P. Johansson, M. Karlsson, Z. Tong, and P. A. Andrekson, "OSNR Requirements for Self-Homodyne Coherent Systems," *IEEE Photonics Technology Letters*, vol. 22, no. 2, pp. 91–93, 2010.
- [74] B. J. Puttnam, J. Sakaguchi, J. M. D. Mendinueta, W. Klaus, Y. Awaji, N. Wada, A. Kanno, and T. Kawanishi, "Investigating self-homodyne coherent detection in a 19 channel space-division-multiplexed transmission link," *Optics Express*, vol. 21, no. 2, pp. 1561–1566, 2013.
- [75] R. S. Luís, B. J. Puttnam, J. M. D. Mendinueta, S. Shinada, M. Nakamura, Y. Kamio, and N. Wada, "Digital Self-Homodyne Detection," *IEEE Photonics Technology Letters*, vol. 27, no. 6, pp. 608–611, 2015.
- [76] E. Le Taillandier de Gabory, M. Arikawa, Y. Hashimoto, T. Ito, and K. Fukuchi, "A Shared Carrier Reception and Processing Scheme for Compensating Frequency Offset and Phase Noise of Space-Division Multiplexed Signals over Multicore Fibers," in *Optical Fiber Communication Conference*, 2013, p. OM2C.2.
- [77] A. J. Viterbi and A. M. Viterbi, "Nonlinear estimation of PSK-modulated carrier phase with application to burst digital transmission," *IEEE Transactions on Information Theory*, vol. 29, no. 4, pp. 543–551, 1983.
- [78] E. Ip and J. M. Kahn, "Feedforward Carrier Recovery for Coherent Optical Communications," *Journal of Lightwave Technology*, vol. 25, no. 9, pp. 2675–2692, 2007.
- [79] T. Pfau, S. Hoffmann, and R. Noé, "Hardware-Efficient Coherent Digital Receiver Concept With Feedforward Carrier Recovery for M-QAM Constellations," *Journal of Lightwave Technology*, vol. 27, no. 8, pp. 989–999, 2009.
- [80] I. Fatadin, D. Ives, and S. J. Savory, "Laser Linewidth Tolerance for 16-QAM Coherent Optical Systems Using QPSK Partitioning," *IEEE Photonics Technology Letters*, vol. 22, no. 9, pp. 631–633, 2010.
- [81] S. K. Oh and S. P. Stapleton, "Blind phase recovery using finite alphabet properties in digital communications," *Electronics Letters*, vol. 33, no. 3, pp. 175–176, 1997.
- [82] T. Pfau and R. Noé, "Phase-Noise-Tolerant Two-Stage Carrier Recovery Concept for Higher Order QAM Formats," *IEEE Journal of Selected Topics in Quantum Electronics*, vol. 16, no. 5, pp. 1210–1216, 2010.

-
- [83] X. Zhou, "An improved feed-forward carrier recovery algorithm for coherent receiver with M-QAM modulation format," *IEEE Photonics Technology Letters*, vol. 22, no. 14, pp. 1051–1053, 2010.
- [84] J. Li, L. Li, Z. Tao, T. Hoshida, and J. C. Rasmussen, "Laser-Linewidth-Tolerant Feed-Forward Carrier Phase Estimator With Reduced Complexity for QAM," *Journal of Lightwave Technology*, vol. 29, no. 16, pp. 2358–2364, 2011.
- [85] X. Li, Y. Cao, S. Yu, W. Gu, and Y. Ji, "A Simplified Feedforward Carrier Recovery Algorithm for Coherent Optical QAM System," *Journal of Lightwave Technology*, vol. 29, no. 5, pp. 801–807, 2011.
- [86] M. Xiang, S. Fu, L. Deng, M. Tang, P. Shum, and D. Liu, "Low-complexity feed-forward carrier phase estimation for M-ary QAM based on phase search acceleration by quadratic approximation," *Optics Express*, vol. 23, no. 15, pp. 19 142–19 153, 2015.
- [87] W. Weber, "Differential Encoding for Multiple Amplitude and Phase Shift Keying Systems," *IEEE Transactions on Information Theory*, vol. 26, no. 3, pp. 385–391, 1978.
- [88] R. Noé, "Phase noise-tolerant synchronous QPSK/BPSK baseband-type intradyne receiver concept with feedforward carrier recovery," *Journal of Lightwave Technology*, vol. 23, no. 2, pp. 802–808, 2005.
- [89] N. R. Newbury, "Searching for applications with a fine-tooth comb," *Nature Photonics*, vol. 5, no. 4, pp. 186–188, 2011.
- [90] C. Liu, J. Pan, T. Detwiler, A. Stark, Y.-T. Hsueh, G.-K. Chang, and S. E. Ralph, "Joint digital signal processing for superchannel coherent optical communication systems," *Optics Express*, vol. 21, no. 7, pp. 8342–8356, 2013.
- [91] D. V. Souto, B.-E. Olsson, C. Larsson, and D. A. A. Mello, "Joint-Polarization and Joint-Subchannel Carrier Phase Estimation for 16-QAM Optical Systems," *Journal of Lightwave Technology*, vol. 30, no. 20, pp. 3185–3191, 2012.
- [92] A. J. Metcalf, V. Torres-Company, D. E. Leaird, and A. M. Weiner, "High-Power Broadly Tunable Electrooptic Frequency Comb Generator," *IEEE Journal of Selected Topics in Quantum Electronics*, vol. 19, no. 6, pp. 231–236, 2013.
- [93] T. J. Kippenberg, R. Holzwarth, and S. A. Diddams, "Microresonator-Based Optical Frequency Combs," *Science*, vol. 332, no. 6029, pp. 555–559, 2011.

Bibliography

- [94] A. Ishizawa, T. Nishikawa, A. Mizutori, H. Takara, A. Takada, T. Sogawa, and M. Koga, "Phase-noise characteristics of a 25-GHz-spaced optical frequency comb based on a phase- and intensity-modulated laser," *Optics Express*, vol. 21, no. 24, pp. 29 186–29 194, 2013.
- [95] M. D. Feuer, L. E. Nelson, X. Zhou, S. L. Woodward, R. Isaac, Benyuan Zhu, T. F. Taunay, M. Fishteyn, J. M. Fini, and M. F. Yan, "Joint Digital Signal Processing Receivers for Spatial Superchannels," *IEEE Photonics Technology Letters*, vol. 24, no. 21, pp. 1957–1960, 2012.
- [96] R. G. H. van Uden, C. M. Okonkwo, V. A. J. M. Sleiffer, M. Kuschnerov, H. De Waardt, and A. M. J. Koonen, "Single DPLL joint carrier phase compensation for few-mode fiber transmission," *IEEE Photonics Technology Letters*, vol. 25, no. 14, pp. 1381–1384, 2013.
- [97] R. S. Luís, B. Puttnam, J. M. Mendinueta, W. Klaus, Y. Awaji, and N. Wada, "Comparing Inter-Core Skew Fluctuations in Multi-Core and Single-Core Fibers," in *Conference on Lasers and Electro-Optics (CLEO)*, 2015, p. SM2L.5.
- [98] G. M. Saridis, B. J. Puttnam, R. S. Luís, W. Klaus, Y. Awaji, and G. Zervas, "Dynamic Skew Measurements in 7, 19 and 22-core Multi Core Fibers," in *OptoElectronics and Communications Conference (OECC)*, 2016, pp. MC2–1.